CHALMERS
UNIVERSITY OF TECHNOLOGY

UNIVERSITY OF GOTHENBURG

# Strong Electron-Phonon Coupling in Graphene

## Investigation of the kink in the $\sigma$-band using a tight binding model

Bachelor thesis in Engineering Physics
Bachelor thesis in Physics


ANDREAS TATIDIS
HENRIK ROHDIN
KRISTOFER NORSTRÖM
OSKAR SJÖKVIST
TIMOTHY HELLBERG
VICTOR WÅHLSTRAND SKÄRSTRÖM

Department of Physics
CHALMERS UNIVERSITY OF TECHNOLOGY
UNIVERSITY OF GOTHENBURG
Gothenburg, Sweden 2017

*Bachelor thesis in Physics 180 HEC*
Henrik Rohdin

*Bachelors thesis in Engineering Physics 180 HEC*
Andreas Tatidis Kristofer Norström Oskar Sjökvist Timothy Hellberg Victor Wåhlstrand Skärström

*Supervisor:* Bo Hellsing
*Examiner at Chalmers:* Lena Falk
*Examiner at University of Gothenburg:* Caroline Beck Adiels

Strong Electron-Phonon Coupling in Graphene:
Investigation of the kink in the $\sigma$-band using a tight binding model

Bachelor Thesis TIFX04-17-34/FYP415.
Department of Physics
University of Gothenburg
SE-411 29 Gothenburg
Telephone +46-31-772 5042

Cover: The simulated kink in spectral function for the $\sigma$-band of graphene near the $\Gamma$ high symmetry point.

Typeset in LaTeX.
Gothenburg 2017

**Abstract**

ARPES experiments show a pronounced kink in the spectral function of the $\sigma$-band in graphene, but its origin has been debated among scientists in the field. One group has found that it may be sublattice interference, a phenomenon inherent to the structure of the graphene unit cell. Recent simulations have showed that the kink can be caused by a strong electron-phonon coupling (EPC) in the region near the $\bar{\Gamma}$-point in the band structure. This bachelor thesis examines the EPC in this region of the band structure, utilising a tight binding model and first order perturbation theory. The simulations were executed in FORTRAN, and the data analysis was done in MATLAB.

Both the $\sigma$ and the $\pi$ scattering processes contribute to the lifetime broadening $\Gamma$ and therefore the spectral function. The $\pi$ scattering is significant but less important, as it makes up 10 % of $\Gamma$ at energies shortly after the kink. The EPC constant at the kink was found to be $\lambda \approx 0.6$. Prior studies have concluded that $\lambda \approx 0.7$ and experiments indicate that $\lambda \approx [0.8, 1.0]$. The transition temperature $T_c$ to superconductivity is calculated to be 23.2 K, which is 26 K lower than previous studies. The lower value of $\lambda$ and subsequently $T_c$ in this thesis is probably a result by the TB model not being as accurate as DFT calculations, but the results of the spectral function still give a qualitatively good result, and indicates that graphene could become superconductive if the Fermi energy might be shifted to the top of the $\sigma$-band.

The tight binding simulation shows a strong kink in the spectral function of the $\sigma$-band, in excellent agreement with the measured function from the ARPES experiment. From this we conclude that the kink ought to foremost be due to elecron-phonon coupling, and not sublattice interference.

Keywords: graphene, tight binding, electron-phonon coupling, solid-state physics

**Sammandrag**

Nyliga ARPES-experiment visar på en tydlig knyck i spektralfunktionen hos $\sigma$-bandet i grafen, men dess ursprung är omdebatterad bland ämneskunniga. En forskargrupp har funnit att knycken skulle kunna tillskrivas undergittersinterferens, ett fenomen som uppkommer på grund av grafens enhetscellsstruktur. Simuleringar har nyligen indikerat att knycken snarare är avhängig stark elektron-fonon-koppling (EPC) nära $\bar{\Gamma}$-punkten i bandstrukturen. Detta kandidatarbete syftar till att undersöka EPC:n i denna region, med hjälp av en metod för starkt bundna elektroner (TB), och första ordningens störningsteori. Simuleringarna genomfördes i FORTRAN, och dataanalysen i MATLAB.

Både $\sigma$- och $\pi$-spridningen bidrar till livstidsbreddningen $\Gamma$, och således också spektralfunktionen. $\pi$-spridningen utgör 10 % precis vid knycken, och är märkbar men mindre viktig i jämförelse med $\sigma$-spridningen som bidrar med 90 %. Kopplingkonstanten vid knycken fanns att vara $\lambda \approx 0.6$. Tidigare studier har påvisat $\lambda \approx 0.7$ och experiment att $\lambda \approx [0.8, 1.0]$. Övergångstemperaturen $T_c$ till supraledning beräknas till 23.2 K, vilket är 26 K lägre än tidigare resultat. De låga värdena på $\lambda$ och $T_c$ i detta arbete är troligen ett resultat av vårt val av den starkt bundna elektron-modellen, vilken inte är lika noggrann som DFT-beräkningar. Resultatet från spektralfunktionen ger dock ett kvalitativt gott resultat, och visar på att grafen skulle kunna bli surpaledande om Fermi-energin kan skiftas ner mot just toppen av $\sigma$-banden.

Våra simuleringar med TB-modellen uppvisar den markanta knycken i spektralfunktionen i $\sigma$-bandet med utmärkt överensstämmelse med den uppmätta ARPES-datan. Vi drar därför slutsatsen att knycken till stor del bör tillskrivas elektron-fonon-koppling, och inte undergitterinterferens.

Nyckelord: grafen, stela jon-approximationen, metoden för starkt bundna elektroner, elektron-fonon-koppling, fasta tillståndets fysik

# Acknowledgements

We would like to thank our supervisor, professor Bo Hellsing at the Department of Physics at University of Gothenburg, for the `FORTRAN` code on which all but a few simulations were executed, without this our work would not have been possible. We would also like to thank Bo for his guidance throughout the project, correcting us when our interpretations led astray and encouraging us to continue on forward, and for the weather reports from San Sebastian.

In addition we would like to thank the C3SE support team, for their invaluable help solving our problems with the ominous FORTRAN language and packages, and the Soliden building for their patience with the bachelor students occupying their cafeteria.

Andreas, Henrik, Kristofer, Oskar, Timothy and Victor
Gothenburg, May 2017

# Contents

# List of Figures

"For groundbreaking experiments regarding the two-dimensional material graphene."

*Andre Geim and Kostya Novoselov were awarded the 2010 Nobel Prize in Physics*

# 1 Introduction

In 2010, the Nobel prize in physics was awarded to Andre Geim and Konstantin Novoselov for their discoveries about graphene. The two Nobel laureates managed to separate layers of graphite by the use of exfoliation through adhesive tape, creating a single layer of carbon. This two-dimensional material came to be known as *graphene*.

Graphene has since its appearance gained momentum in the scientific sphere. Recent studies of graphene has shown a kink in the $\sigma$-band, which has led to speculations regarding potential superconductivity by utilising this band which has a theoretical electron-phonon coupling constant of up to $\lambda = 0.7$. This is supported by experiment with values up to $\lambda = 1.0$ [1]. Graphene is not a natural superconductor, and the $\pi$-band at the Fermi energy has a low value of $\lambda$. A potential possibility would be to lower the Fermi level from the $\pi$-band to the $\sigma$-band in order to utilise its transportability of electrons, and possibly making it superconductive [2]. The conclusion of this material is stated as follows, that the future of graphene lies in its many interesting properties - which are plentiful.

## 1.1 Graphene

Graphene is a single layer two-dimensional material with a honeycomb lattice and is one of the building block of larger constellations in the carbon family; diamond and graphite (3D), graphene (2D), carbon nanotubes (1D) and fullerenes (0D). Graphene was the first 2D material to be discovered outside the theoretical realm. The fabrications of graphene are various, though the best way to generate the highest purity today is by exfoliation[3]. However, errors in the fabrication process of graphene occur naturally, leading to deterioration of its properties.

As mentioned earlier, graphene has a wide range of properties interesting to science and engineering, a few of which will be covered: By testing the strength of graphene through nanoindentention it was shown to be the strongest material ever measured at the time (2008) [4]. It is also transparent, and has been able to act as

a transparent conductor in solar cells [5]. Graphene has successfully been used as a filter to separate saltwater into fresh water [6]. Single layered graphene exhibits an extraordinary heat conductivity, ranging between 4.84 and 5.30 kW/mK [7]. This property would make graphene an excellent material for thermal management in components.

Graphene is a semimetal with zero band gap and high electroconductivity, comparable to copper [8]. By examining the electric properties of the band structure, it becomes evident that there are few energy states near the Fermi energy. This makes the electron-phonon coupling, the dominating effect in low temperature superconductivity, very weak.

## 1.2 Recent Investigations

Recent findings from ARPES experiments show that there is a kink in the $\sigma$-band.[2] The origin of the kink could be due to sublattice interference [9] or to electron-phonon coupling in the $\sigma$-band [1]. The latter argument is made from an article published 2017, in which first principle studies were used to determine that the electron phonon coupling is the underlying component of the kink. Because the EPC in the $\sigma$-band was found to be considerably stronger than in the energetically higher lying $\pi$-band, the result is interesting if the Fermi level could be shifted to the $\sigma$-band. The $\sigma$-band also has a much higher density of states, which would yield a better conductive ability at higher temperatures.

## 1.3 Purpose and Scope of the Thesis

The main purpose of this thesis is to theoretically investigate the kink in the spectral function of graphene observed in the ARPES experiment using numerical simulations. More specifically, the *electron-phonon coupling* (EPC) is used to calculate the spectral function to emulate the ARPES data, and the contributions from the different phonon modes are examined. With an elementary understanding of the EPC in the outer $\sigma$-band of graphene, we are able to calculate approximately the EPC coupling parameter $\lambda$ and transition temperature $T_c$ using Migdal-Eliashberg theory. These are the important parameters relating to superconductivity which constitutes the secondary purpose of this thesis.

In order to construct the spectral function from EPC, it is necessary to calculate the electronic band structure and the single electron wave function of graphene, and subsequently the lifetime broadening $\Gamma$ of the electronic band states. The band structure and the approximate electron wave function are calculated using a tight binding model where we only consider nearest neighbour interactions and neglect the overlap matrix. The lifetime broadening is determined using first order time-dependent perturbation theory where the Hamiltonian is modelled as a Gaussian

potential. We make our calculations in a low temperature environment, as this means no characteristic phonon modes can exist in the graphene. The validity of our assumptions, approximations and models are discussed and analysed, not only by comparing our results to the ARPES experiment but also by varying one of the potential parameters to see how sensitive our model is.

# 2 Theory

This chapter explains the necessary theoretic framework to describe the electron-phonon coupling in a crystalline material with hexagonal lattice symmetry, such as graphene. First the electronic band structure is explained through a tight binding approximation, which is needed to describe the allowed energy states of the electrons in the solid. Next, the concept of phonons is explained which is the fundamental phenomenon that interacts with the electron states, giving rise to the electron-phonon coupling. It is further explained how this coupling can be quantified by measuring its influence on the lifetime of empty electron states, which in turn is connected to the self-energy in the system. The self-energy can be calculated from the spectral function, which is the expected data from an ARPES experiment.

Furthermore, the electron-phonon coupling is related to superconductivity according to McMillan's formula originating in Migdal-Eiashberg theory, which is described in the last section of this chapter.

## 2.1 Tight Binding

The *tight binding* (TB) approximation relies heavily on the principle of superposition, where atomic orbitals are taken as a basis for further computation of electronic properties in solids. This section explains the basic concepts for solid state calculations and in particular the TB model. The symmetry of atoms in the crystal affects the Hamiltonian in the Schrödinger equation, which can be solved with a linear combination of atomic orbitals as eigenfunctions. This Schrödinger equation is solved in the tight binding model as the secular equation in Section 2.1.4.

### 2.1.1 The Unit Cell and the First Brillouin Zone

The structure of a 2-dimensional crystalline solid can be modelled as a repeating pattern of atoms, which can be divided into *unit cells*; equal sections of space that have some degree of rotational and translational symmetry that when laid side by side describe the whole crystal [10:8]. In graphene, the unit cell is constructed by pairing two atoms next to each other together to form a basis, after which the unit cell is taken to have a rhombic shape, with $\pi$-rotational symmetry, see Figure 1. This is specifically the hexagonal Bravais lattice, where the *lattice vectors* $\mathbf{a}_i$ points at *lattice points* located in the centre of each hexagon. Each unit cell is associated with exactly one lattice point, defining the *primitive* unit cell.

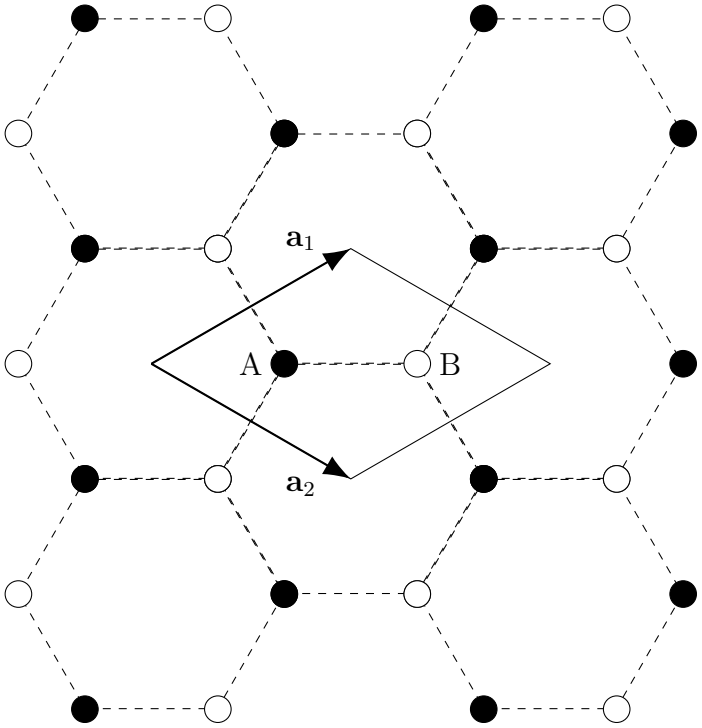


Figure 1: *Crystal structure of graphene with the unit cell encompassing the two basis atoms A and B. The lattice vectors are* $\mathbf{a}_1$ *and* $\mathbf{a}_2$*, and the lattice point associated with the unit cell is located in the corner to the left in the cell.*

The lattice vectors $\mathbf{a}_1, \mathbf{a}_2$ spanning the unit cell can be transformed to the *reciprocal space* by choosing their relation to the *reciprocal lattice vectors* $\mathbf{G}_1, \mathbf{G}_2$ as

$$\mathbf{a}_i \cdot \mathbf{G}_j = 2\pi\delta_{ij}. \tag{1}$$

The reciprocal space can be thought of as an analog to the Fourier space; it contains the wave vectors of waves in the lattice. In reciprocal space the reciprocal lattice vectors point, in the same way to the regular lattice vectors, at reciprocal unit cells. *The first Brillouin zone* (1BZ) is the primitive unit cell in reciprocal space, which for real spaced unit cell defined as in Figure 1 creates a hexagonal primitive unit cell in reciprocal space as in Figure 2. The centre point of 1BZ is called the $\bar{\Gamma}$-point, and in a hexagonal symmetry there are two other points called the $\bar{\mathrm{K}}$-point and the $\bar{\mathrm{M}}$-point that together label the shape and symmetry of the 1BZ. The 1BZ contains all of the allowed wave vectors in the crystal, the reason for this will be further explained in subsequent chapters.

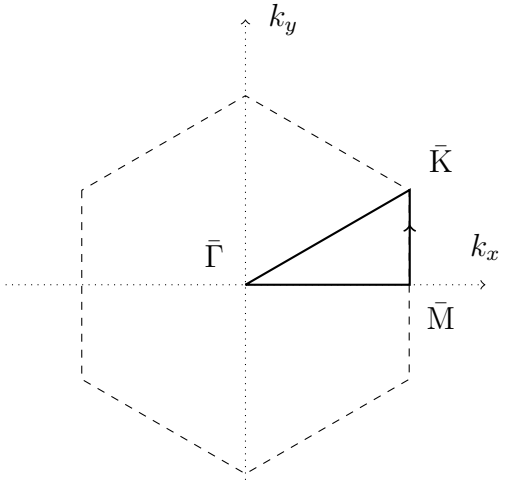


Figure 2: *The first Brillouin zone (1BZ) of the reciprocal hexagonal lattice of graphene.* $k_x, k_y$ *labels the x and y components of wave vectors in the reciprocal space.* $\bar{\Gamma}, \bar{\mathrm{K}}, \bar{\mathrm{M}}$ *are the symmetry points defined by the edges of the triangle in the figure.*

### 2.1.2 Slater's Approximation and Atomic Orbitals

If there are more than two electrons in an atom, the electrons interact not only with the Coulomb field of the protons in the nucleus, but with each others Coulomb fields as well. The instantaneous interaction between two such electrons is complicated, but the statistical effects of such interactions can be quantified by introducing a *screened core charge*. This takes into account that electrons in orbitals closer to the nucleus screen the Coulomb field of the nucleus to the other electrons. Given an electron orbital wave function $\phi$, it can be separated into two parts: a radial part $R_{nl}$ which describes the radial distribution of the wave function, and an angular part $Y_{\ell m}$ which describes the angular distribution. The radial part of the wave function can be approximated as a *Slater Type Atomic Orbital* with features close to the analytically derived radial hydrogenic electron wave function, except without radial nodes [11:398]. Its mathematical form is

$$R_{Slater}(r) = Nr^{n-1}e^{-\zeta_n r} \tag{2}$$

where $r$ is the position vector, $N$ a normalization constant, $n$ the quantised electron energy level and $\zeta_n$ the screened core charge. The value of $\zeta_n$ can be derived by the semi-empirical *Slater's rule*, which give the relevant effective core charge for carbon to be $\zeta_{2s,2p} = 3.25$ [12:58]. Note that equation (2) lacks dependency on $\ell$. This is because the radial nodes close to the nucleus are being omitted, as Slater type orbitals are used to approximate the behaviour of electrons some distance

from the nucleus. The value of the normalization constant is given by

$$N = \frac{(2\zeta_n)^{n+1/2}}{\sqrt{(2n)!}}. \tag{3}$$

Slater's rule is valid for determining the screening constant for electrons in light elements with up to d shells, such as carbon [12].

Carbon has only two valence orbitals, namely the $2s$ and $2p$ orbitals. The $p$ orbital may be decomposed into a linear combination of three orthogonal wave functions $p_x, p_y, p_z$. These atomic orbitals are drawn in Figure 3. The decomposi-

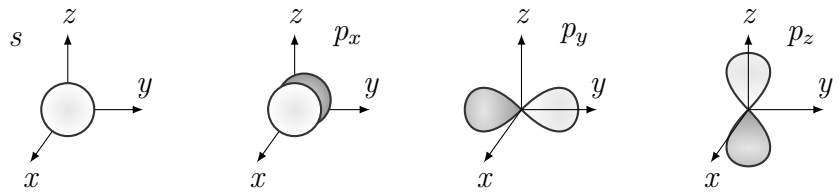


Figure 3: *The relevant valence electron atomic orbitals in carbon and boron. The $s$ orbital is spherically symmetrical along all axes, whereas the $p$ orbital has three components $p_x, p_y, p_z$, symmetrical around their respective axis.*

tion also illustrates the mutual orthogonality of the orbitals, in Dirac notation this is

$$\begin{aligned} \langle 2p_i | 2p_j \rangle &= \delta_{ij} \\ \langle 2s | 2p_i \rangle &= 0, \, \forall i \end{aligned} \tag{4}$$

where $\delta$ is the Kronecker delta. The orthogonality also holds for modification of orbitals under an operator $\hat{H}_k$ along a binding axis $k$:

$$\begin{aligned} \langle 2p_i | \, \hat{H}_k \, | 2p_j \rangle &\propto \delta_{jk}\delta_{ik} \\ \langle 2s | \, \hat{H}_k \, | 2p_i \rangle &\propto \delta_{ik}, \end{aligned} \tag{5}$$

which in short means that if the operator $\hat{H}_k$ does not act in the same direction as the $p$ orbital, its contributions are neglected.[13]

### 2.1.3 Bloch's Theorem and the Electron's Total Wave Function

The Bloch theorem states that the eigenfunction $\Phi$ of a periodic potential is the product of a periodic function and a plane wave [10:167];

$$\Phi(\mathbf{r}, \mathbf{k}) = e^{i(\mathbf{k}\cdot\mathbf{r})} u_{\mathbf{k}}(\mathbf{r}) \tag{6}$$

where $u_{\mathbf{k}}(\mathbf{r})$ has the same periodicity as the lattice, $\mathbf{k}$ is any wave vector inside 1BZ and $\mathbf{r}$ is the position vector. The Bloch wave is a lattice eigenfunction because it is invariant under any translation by any lattice vector $\mathbf{r} + \mathbf{a}$, and is only phase shifted by $\exp(\mathbf{G} \cdot \mathbf{r})$ for any $\mathbf{k}' = \mathbf{k} + \mathbf{G}$ outside the 1BZ [14:166].

The atomic wave functions $\phi_j$ of types $j$ model the behaviour of the electrons around the atoms, and are therefore used as basis for the eigenfunction $\Phi$ for the lattice. The atomic orbitals of interest are those that carry the valence electrons, which are the $2s, 2p_x, 2p_y$ and $2p_z$ orbitals in carbon, where the $2p$ orbitals have identical radial parts, see Figure 3.

An eigenfunction $\Phi$ for the lattice can be constructed by summation of atomic orbitals, and keeping the Bloch theorem in mind,

$$\Phi_{j,s}(\mathbf{r}, \mathbf{k}) = \frac{1}{\sqrt{N}} \sum_{\mathbf{R}_s}^{N} e^{i\mathbf{k}\cdot\mathbf{R}_s} \phi_{j,s}(\mathbf{r} - \mathbf{R}_s) \tag{7}$$

where $s$ is the site for the atom $A$ or $B$, $\sqrt{N}$ is a normalisation constant [15:2], $\mathbf{R}_s$ is a lattice vector pointing to the origo in any other unit cell, the sum is taken over all unit cells in the crystal, and the phase factor ensures that the phase is correct as in equation (6) if we choose any point $\mathbf{r} + \mathbf{a}$ in any other unit cell;

$$\begin{aligned} \Phi_{j,s}(\mathbf{r} + \mathbf{a}, \mathbf{k}) &= \frac{1}{\sqrt{N}} \sum_{\mathbf{R}_s}^{N} e^{i\mathbf{k}\cdot\mathbf{R}_s} \phi_{j,s}(\mathbf{r} + \mathbf{a} - \mathbf{R}_s) = \\ &= \frac{1}{\sqrt{N}} e^{i\mathbf{k}\cdot\mathbf{a}} \sum_{\mathbf{R}_s - \mathbf{a}}^{N} e^{i\mathbf{k}\cdot(\mathbf{R}_s - \mathbf{a})} \phi_{j,s}(\mathbf{r} - (\mathbf{R}_s - \mathbf{a})) = e^{i\mathbf{k}\cdot\mathbf{a}} \Phi_{j,s}(\mathbf{r}, \mathbf{k}) \end{aligned} \tag{8}$$

where $\mathbf{a}$ is defined as in Section 2.1.1. The summation is shifted with a lattice vector, because the same type of orbital $\phi_j$ can be found in any unit cell because of the crystal symmetry. This also holds for any addition of a reciprocal lattice vector $\mathbf{G}$ to any other Brillouin zone,

$$\Phi_{j,s}(\mathbf{r}, \mathbf{k} + \mathbf{G}) = \frac{1}{\sqrt{N}} \sum_{\mathbf{R}_s} e^{i(\mathbf{k}+\mathbf{G})\cdot\mathbf{R}_s} \phi_{j,s}(\mathbf{r} - \mathbf{R}_s) = e^{i\mathbf{G}\cdot\mathbf{R}_s} \Phi_{j,s}(\mathbf{r}, \mathbf{k}). \tag{9}$$

Note that $\mathbf{G} \cdot \mathbf{R}_s = 2\pi$ and that exponential is 1 by definition in equation (1). These orbitals can be combined into a superposition of all Bloch waves $\Phi_j$ of every orbital type $j$,

$$\psi(\mathbf{r}, \mathbf{k}) = \sum_{j,s} c_{s,j} \Phi_{j,s}(\mathbf{r}, \mathbf{k}). \tag{10}$$

This function $\psi_{n,\mathbf{k}}$ is the total lattice wave function and is an eigenfunction to the lattice potential. The eigenfunction $\psi(\mathbf{r}, \mathbf{k})$ is thus a linear combination of Bloch orbitals.

### 2.1.4 The Secular Equation

The graphene lattice has a system Hamiltonian $\hat{H}$ and a total wavefuntion which is assumed to be given by equation (10). From here on, the notion that the wave function is a function of $\mathbf{k}$ and $\mathbf{r}$ will be omitted as it is not important in the derivation of the secular equation. However, an index $\mathbf{k}$ will be written on the energy eigenvalue $\varepsilon_{\mathbf{k}}$ as a reminder. Note that the indices $s, j$ in equation (10) can be simplified to a single index $i$ by arranging the terms in an orderly way. Next, the variational method of finding the energy eigenvalues is used. This is given as

$$\varepsilon_{\mathbf{k}} \leq E_{\mathbf{k}} = \frac{\langle \psi | \hat{H} | \psi \rangle}{\langle \psi | \psi \rangle} \tag{11}$$

with an equal-sign if and only if the wave function is the eigenfunction to the Hamiltonian. Inserting the expression for $\psi$ given in equation (10) with the indices simplified gives

$$\varepsilon_{\mathbf{k}} = \frac{\sum_{i,i'} c_i^* c_{i'} \langle \Phi_i | \hat{H} | \Phi_{i'} \rangle}{\sum_{i,i'} c_i^* c_{i'} \langle \Phi_i | \Phi_{i'} \rangle} = \frac{\sum_{i,i'} c_i^* c_{i'} H_{ii'}}{\sum_{i,i'} c_i^* c_{i'} S_{ii'}} \tag{12}$$

where $H_{ii'} = \langle \Phi_i | \hat{H} | \Phi_{i'} \rangle$ and $S_{ii'} = \langle \Phi_i | \Phi_{i'} \rangle$. This equation is minimized with respect to the constants $c_i^*$. The following derivation may seem unintuitive at first glance, but remember that the derivation is with respect to a single variable at a time, so pay attention to what happens with the summation indices. For clarity, the derivation index is changed to $n$ which denotes a specific $i$:

$$
\begin{aligned}
\frac{\partial \varepsilon_{\mathbf{k}}}{\partial c_n^*} &= \frac{\partial}{\partial c_n^*}\left(\frac{\sum_{i,i'} c_i^* c_{i'} H_{ii'}}{\sum_{i,i'} c_i^* c_{i'} S_{ii'}}\right) \\
&= \frac{\sum_{i'} c_{i'} H_{ni'}}{\sum_{i,i'} c_i^* c_{i'} S_{ii'}} - \left(\frac{\sum_{i,i'} c_i^* c_{i'} H_{ii'}}{\sum_{i,i'} c_i^* c_{i'} S_{ii'}}\right) \cdot \frac{\sum_{i'} c_{i'} S_{ni'}}{\sum_{i,i'} c_i^* c_{i'} S_{ii'}} \\
&= \frac{\sum_{i'} c_{i'} H_{ni'} - \varepsilon_{\mathbf{k}} \cdot \sum_{i'} c_{i'} S_{ni'}}{\sum_{i,i'} c_i^* c_{i'} S_{ii'}} = 0 \Leftrightarrow \\
&\Leftrightarrow \sum_{i'} c_{i'} H_{ni'} - \varepsilon_{\mathbf{k}} \sum_{i'} c_{i'} S_{ni'} = 0.
\end{aligned}
\tag{13}
$$

There is one equation for every index $n$, thus all equations given by equation (13) can be written on matrix form,

$$
H\mathbf{c} - \varepsilon_{\mathbf{k}} S\mathbf{c} = (H - \varepsilon_{\mathbf{k}} S)\mathbf{c} = 0. \tag{14}
$$

This equation will only have non-trivial solutions when the determinant of the matrix equals to zero,

$$
\det(H - \varepsilon_{\mathbf{k}} S) = 0. \tag{15}
$$

This is the secular equation. The solutions of this equation gives all energy eigenvalues of the Hamiltonian of the system. These eigenvalues are, as stated earlier however omitted, dependent on $\mathbf{k}$.

## 2.2 Band Structure

The band structure describes the energy states $\varepsilon$ of the electrons in a crystalline solid, computed from equation (15), based on their wave vectors $\mathbf{k}$. These $\varepsilon$ are often plotted along certain paths in the 1BZ, such as between the $\bar{\Gamma}$, $\bar{\mathrm{K}}$ and $\bar{\mathrm{M}}$ points in graphene, which is called the *high symmetry line* [14:64]. The plot along the path is the *band structure* of the material, as the degeneracy of $\varepsilon$ on $\mathbf{k}$ creates bands along the high symmetry line.

Every pair of $\varepsilon$ and $\mathbf{k}$ signifies a unique electron state $\varepsilon_{n,\mathbf{k}}$ in the crystal, where $n$ denotes which band the electron state is in. The relevant bands for this work is the $\pi$-band and the two lower lying $\sigma$-bands, see Figure 10. In a solid at zero Kelvin, the electrons will fill up the states up to an energy level $\varepsilon_F$ called the *Fermi energy*, because the fermionic electrons obey the Pauli exclusion principle.

The two most important bands for the electronic properties of a crystalline solid are the valence band and the conduction band. The valence band is the energetically highest lying band in the structure with occupied electron states in

it. The conduction band is situated energetically above the conduction band, but it has no occupied states. Crystalline materials usually have an energy gap between these bands where there are no states that the electrons can occupy. In graphene there is no such gap as these bands overlap at the $\bar{\text{K}}$-point, see Figure 10. This means that electrons in the lower lying valence $\pi$-band can be excited above the Fermi energy by thermal photons, up to the next (empty) conduction $\pi$-band. The density of electronic states is related to the energy bands such that the density is higher at the flat parts[14:177].

## 2.3 Phonons

Phonons are the quantisation of vibrations of the atoms in the crystal lattice, which mediate sound, thermal, and electrical conductivity. The phonon can be thought of as a travelling displacement wave in the crystal lattice, with wave vector $\mathbf{q}$ and frequency $\omega$, sprung from the Coulomb interaction between the atoms in the crystal.

### 2.3.1 One Dimensional Dispersion Example

The relation between a chain of vibrating atoms can be classically modelled as point masses connected by springs. In this model, the frequency $\omega$ is nonlinear to the wave vector $\mathbf{q}$, and have to be calculated through its dependency on the force between the atoms. Consider an atom at site $s$ in a interconnected string of atoms, then the force affecting the atom is

$$F = K(u_{s+1} - u_s) + K(u_{s-1} - u_s) \tag{16}$$

with $K$ being the spring constant between the atoms and $u_s$ the displacement of the atom at site $s$ [10:91]. The interaction of next-nearest neighbours is neglected because the displacements $u_i$ are considered small. Through Newtons second law and equation (16) one can derive the *dispersion relation*, which is the equation that describes the allowed phonon frequencies in the string,

$$\omega(q) = (2K/M)(1 - \cos(qd)) \tag{17}$$

where $q$ is the wave number of the phonon, $d$ is the distance between neighbouring atoms, and $M$ the mass of an atom, see [10:92] for a complete derivation of this relation. Because the smallest distance between two atoms is $d$, this limits the smallest phonon wave length to be $2d$ according to the Nyqvist theorem, and thus phonons outside 1BZ lacks physical meaning [16:63].

### 2.3.2 Phonon Characteristics

The phonon can vibrate the atoms in modes either in or out of phase relative to each other. An optical vibration $O$ has the atoms moving out of phase, and in phase for an acoustic vibration $A$. Given the crystal plane, phonon waves can move in a transverse $T$, longitudinal $L$ and out of plane $Z$ waves giving rise to a total of six different modes $\nu$ in conjunction to the two phase movements.

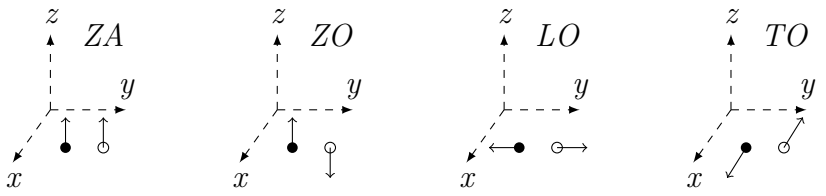


Figure 4: *The four dominant modes of the phonon vibrations in graphene. The $L/T/Z$ modes are distinguished by the direction of oscillation in $x, y, z$, and optical or acoustical modes are in our out of phase, respectively. The wave vector* $\mathbf{q}$ *is pointing in the $y$-direction.*

The energy content $\varepsilon_\nu$ of a phonon mode $\nu$ is quantised and can be calculated by

$$\varepsilon_\nu = \left(n + \frac{1}{2}\right)\hbar\omega_\nu \tag{18}$$

where $n$ is the number of phonons in the mode. Different modes of vibration $\nu$ carry different energy, this is because different modes give rise to different dispersion relations.

Some phonon modes contribute more to the electron-phonon coupling compared to others. The $TA$ and $LA$ modes have a near-zero contribution compared to their optical counterparts $TO, LO$, and similarly the $ZO$ mode is negligible compared to $ZA$. The contributing modes can be seen in Figure 4. In addition, the energy scale of the phonon dispersion reveals that $\omega_{LO}$ is approximately equal to $\omega_{TO}$, and this energy is denoted as $\Omega = 175\,\text{meV}$ for all $\mathbf{q}$ near the $\bar{\Gamma}$-point.[17]

Phonons are bosons and therefore their occupancy is given by the Planck distribution [10:107];

$$\langle n\rangle = \frac{1}{\exp(\hbar\omega_\nu/k_BT) - 1} \tag{19}$$

where $\langle n\rangle$ is zero at very low temperatures, i.e. no phonon vibrations can exist at very low temperatures.

## 2.4 Electron-Phonon Coupling

In low temperature environments there are no characteristic phonon modes, as made evident in equation (19), if not excited externally. Empty *hole states* can be created by photo emission, when a photon excites an electron so that it leaves the material, thus creating a state which can be filled by an electron from an energetically higher state. Equilibrium is achieved by the system if an electron in

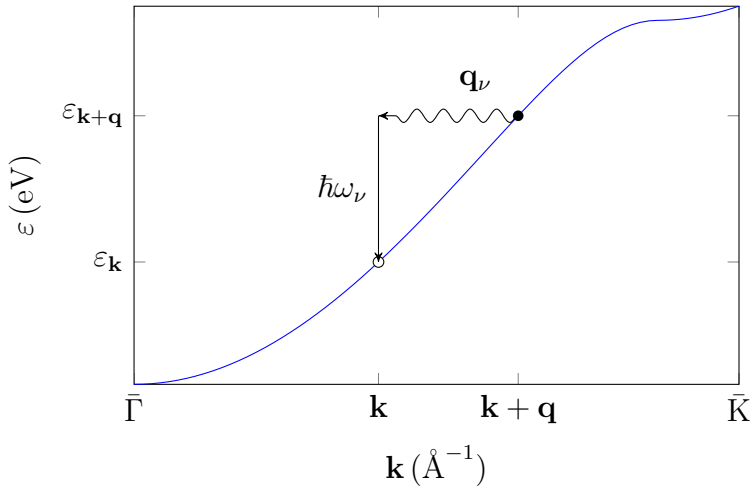


Figure 5: *Demonstration of the conservation of energy and momentum of electron hopping with an excited phonon. The electron assumes an energy state* $\varepsilon_{\mathbf{k}'}$ *by means of a phonon with crystal momentum* $\mathbf{q}$.

a higher energy $\varepsilon_{\mathbf{k}'}$ state emits a phonon that carries away the right amount of energy and crystal momentum, such that the electron may occupy the hole state $\varepsilon_{\mathbf{k}}$. This process is the interpretation of *electron-phonon coupling* in this thesis. The emitted phonon must thus conserve both crystal momentum and energy in the system, giving rise to two constraints for the phonon wave vector $\mathbf{q}$ and its energy $\varepsilon_{\mathbf{q}}$, see Figure 5;

$$\begin{aligned} \mathbf{k}' &= \mathbf{k} + \mathbf{q} \\ \varepsilon_{\mathbf{k}'} &= \varepsilon_{\mathbf{k}} + \varepsilon_{\mathbf{q}} \end{aligned} \tag{20}$$

where $\mathbf{k}', \mathbf{k}$ denotes the final and initial electron states respectively. The phonon energy in turn is quantised in terms of its dispersion $\omega$ in equation (18), such that $\varepsilon_{\mathbf{q}} = \hbar\omega$ .

Crystal momentum can be defined for a electron wave packet as $\hbar\mathbf{k}$ [10:173], given the wave vector in equation (9), and as $\hbar\mathbf{q}$ for phonons. Crystal momentum is a conserved quantity in the 1BZ up to a reciprocal lattice vector $\mathbf{Q}$[16:121].

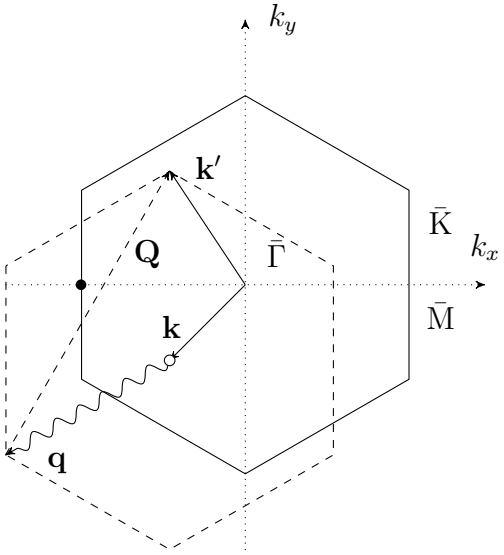


Figure 6: *High-momentum electrons* $\mathbf{k}' = \mathbf{k} + \mathbf{q}$ *can be transferred into the 1BZ by means of a reciprocal lattice vector* $\mathbf{Q}$*, meaning crystal momentum is conserved. This process is call Umklapp scattering.*

High-momentum phonons or electrons can due to the peridocity of the lattice be transferred back into the 1BZ, see Figure 6. This process is called *Umklapp scattering*.

The periodicity in the lattice means that all types of wave vectors in the crystal can be described by the vectors inside 1BZ [16:62], as any addition of a reciprocal lattice vector only adds a phase factor to the travelling wave. The implication of this fact is that wave vectors are a conserved quantity in the lattice.

### 2.4.1 Transition Rates and Lifetime Broadening

We are interested in these hopping events and the coupling, and aim to describe it by means of the transition rate $\Gamma$, also known as the lifetime broadening. Heisenberg's uncertainty principle states that

$$\Delta E \Delta t \gtrsim h \tag{21}$$

where $\Delta E, \Delta t$ are small changes in energy and time of a state, respectively. We take $\tau$ as the mean lifetime of a state and define the lifetime broadening $\Gamma$ :

$$\Delta E \approx \frac{h}{\tau} \equiv h\Gamma. \tag{22}$$

The lifetime broadening is as such a measure of the energy variation near the bounds of the Heisenberg uncertainty principle.

One may now relate the lifetime broadening to an initial state $|i\rangle$ and a final state $|f\rangle$ by means of the famous Fermi's Golden Rule:

$$\Gamma_{i\to f} = \frac{2\pi}{\hbar}\Big|\langle f|\hat{H}|i\rangle\Big|^2\rho \tag{23}$$

The equation describes the transition rate from states $i \to f$, and is dependent upon the transition constant matrix element $\langle f|\hat{H}|i\rangle$ and the energy density of final states $\rho$.
By applying Fermi's Golden Rule to our coupled system, the total transition constant is $|\langle n\mathbf{k}|H+\delta V|n'\mathbf{k}+\mathbf{q}\rangle|^2$ between two states with momentum $\mathbf{k}$ and $\mathbf{k}' = \mathbf{k}+\mathbf{q}$. We define $\delta V$ as the perturbation of the system Hamiltonian due to the electron-phonon coupling, modelling the phonon distortion to the lattice potential felt by the electrons. The lifetime broadening energy due to just EPC is therefore on the form [18]

$$\Gamma_{n\mathbf{k}} = 2\pi\sum_{n'\nu\mathbf{q}}\Big|\langle n\mathbf{k}|\delta V^{\nu}_{\mathbf{q}}|n'\mathbf{k}+\mathbf{q}\rangle\Big|^2\delta(\varepsilon_{n'\mathbf{k}+\mathbf{q}}-\varepsilon_{n\mathbf{k}}-\hbar\omega_{\nu\mathbf{q}}) \tag{24}$$

where the $\delta$ factor assures that the energy conservation of equation (20) is satisfied. Since we only consider states where $\mathbf{k}' = \mathbf{k}+\mathbf{q}$, crystal momentum is conserved by construction.

## 2.5 The Spectral Function

The experimental observable corresponding to the lifetime broadening $\Gamma$ is known as the *spectral function*, $A = A(\varepsilon)$, constructed theoretically by means of Green's functions.

In its most simple form, a Green's function can be described as a single electron state. The Green's function of the single state $|a\rangle$ is written as

$$G_a(\varepsilon) = \frac{1}{\varepsilon-\varepsilon_a-i\gamma} \tag{25}$$

where $\varepsilon_a$ is the energy of the state and $\gamma$ is a positive infinitesimal. The spectrum of the Green's function can be expressed as the probability that the electron has the energy $\varepsilon$ [19], and it is given by the imaginary part of the normalized system Green's function. The spectrum of the system described by equation (25) is thus given by

$$A(\varepsilon) = \frac{1}{\pi}\operatorname{Im}G_a = \frac{1}{\pi}\frac{\gamma}{(\varepsilon-\varepsilon_a)^2+(\gamma)^2} \to \delta(\varepsilon-\varepsilon_a), \tag{26}$$

where $\delta$ is the delta-function when $\gamma \to 0$. This means that the spectrum of this Green's function is equivalent to a state with energy at $\varepsilon_a$, nothing previously unknown however made very evident.

Consider the state $|a\rangle$ coupled to for example phonons. This corresponds to replacing the $i\gamma$ in the denominator with a complex so called *self-energy*, denoted by $\Sigma_a(\varepsilon)$. The self-energy is the contribution to the energy (effective mass) of a particle caused by interactions between the particle and the system it's a part of. The coupled Green's function is given by

$$G_a = \frac{1}{\varepsilon - \varepsilon_a - \Sigma_a(\varepsilon)} \tag{27}$$

and has the spectrum according to equation (26)

$$A_a(\varepsilon) = \frac{1}{\pi} \frac{\operatorname{Im} \Sigma_a(\varepsilon)}{(\varepsilon - \varepsilon_a - \operatorname{Re} \Sigma_a(\varepsilon))^2 + (\operatorname{Im} \Sigma_a(\varepsilon))^2}. \tag{28}$$

In the band picture, we label the states $a$ with band index $n$ and electron momentum $\mathbf{k}$, and so the spectral function is thus given by

$$A_n(\varepsilon, \mathbf{k}) = \frac{1}{\pi} \frac{\operatorname{Im} \Sigma_n(\varepsilon, \mathbf{k})}{(\varepsilon - \varepsilon_n(\mathbf{k}) - \operatorname{Re} \Sigma_n(\varepsilon, \mathbf{k}))^2 + (\operatorname{Im} \Sigma_n(\varepsilon, \mathbf{k}))^2}. \tag{29}$$

### 2.5.1 Angle-Resolved Photoemission Spectroscopy, ARPES

For the past 20 years, angle-resolved photoemission spectroscopy (ARPES) has become a widely recognised method for its ability to directly measure the distribution of electrons in the reciprocal lattice of solids. It is, as the name implies, a method utilising photoemission. A photon is absorbed by the sample and if the photon supplied sufficient energy, the sample emits an electron. A detector equipped with an energy filter captures the emitted electron within a certain energy range and in a certain solid angle. Using conservation of momentum and energy, one can deduce information about the electron's initial momentum, energy and lifetime. In the sudden approximation, ARPES data can be seen as the direct measurement of the single-particle spectral function $A(\varepsilon, \mathbf{k})$. [20], [21]

Previous experiments and analyses have documented that the $\sigma_o$-band in graphene has a distinctive kink at approximately $-0.2\,\mathrm{eV}$ relative to the top of the band, see Figure 7. Different explanations have been attributed to it, amongst them sublattice interference and EPC.

### 2.5.2 Self-energy $\Sigma$ and its Connection to Lifetime Broadening

The self-energy is, as described earlier, the contribution to the energy of a particle due to interactions with the surroundings. Consider an electron in a lattice. It has an energy on its own, but it also affects the surrounding lattice by pulling the

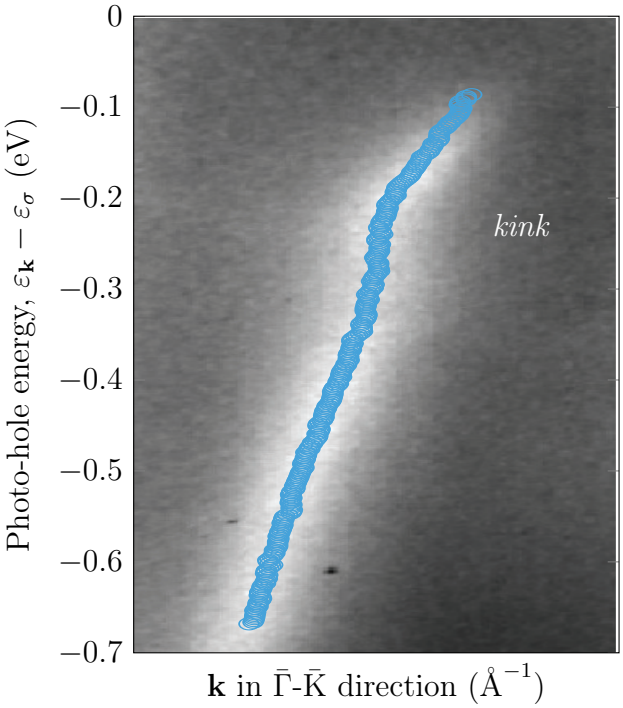


Figure 7: *ARPES experimental data of the electron distribution in the top $\sigma$-band. The so called kink is clearly visible at around $-0.2\,\mathrm{eV}$, relative to the top of the band. The picture was taken from [1] with the permission of the authors.*

lattice closer. This modifies the potential, which in turn modifies the energy of the electron. It is in fact related to the lifetime broadening by the relation[22]

$$\text{Im } \Sigma_a = \frac{1}{2}\Gamma. \tag{30}$$

To obtain a clear physical interpretation of the lifetime broadening, it is of interest to transform the Green's function from the frequency domain to the time domain. Since the self-energy is a complex function, this can be written as a sum of its real and imaginary components. Writing out the Green's function gives

$$G_a(\varepsilon) = \frac{1}{\varepsilon - \varepsilon_a - \text{Re } \Sigma_a - i\,\text{Im } \Sigma_a}. \tag{31}$$

and transforming this into the time domain gives

$$G_a(t) \propto e^{-i(\varepsilon_a + \text{Re } \Sigma_a)(t-t_0)} e^{-\text{ Im } \Sigma_a (t-t_0)}. \tag{32}$$

In the second factor, one may notice a decay term. Thus, the decay rate of state $a$ is proportional to the imaginary part of the self energy, i.e the lifetime broadening. [23] There is a relation between the real and the imaginary part of complex

functions known as the *Kramers-Kronig relation*. This requires the function to be analytic in the upper half plane, a condition automatically satisfied by response functions of stable systems[24]. Since the Green's function described in equation (31) is a response function, it satisfies the condition required, and the complex parts of the self-energy are thus related such that

$$\text{Re } \Sigma(\varepsilon) = \frac{1}{\pi}\mathcal{P}\int \frac{\text{Im } \Sigma}{\varepsilon' - \varepsilon} d\varepsilon' \tag{33}$$

where $\mathcal{P}$ denotes that the integral is the Cauchy principal value integral [25]. This implies that the self-energy can be described in terms of the lifetime broadening, and furthermore, the spectral function.

## 2.6 Eliashberg Function $\alpha^2F(\omega)$

The Eliashberg function yields almost all of the characteristics of the electron-phonon coupling, and it is defined as the electron-phonon spectral function. At low temperatures where only phonon emission takes place, it is given by

$$\alpha^2F(\omega) = \frac{1}{N(0)} \sum_{n\mathbf{k},n'\mathbf{k+q},\nu} |g^{\nu}_{n\mathbf{k},n'\mathbf{k+q}}|^2 \delta(\varepsilon_{\mathbf{k}} - \varepsilon_{\mathbf{k+q}} - \hbar\omega^{\nu}_{\mathbf{q}})\delta(\omega - \omega^{\nu}_{\mathbf{q}}) \tag{34}$$

where $N(0)$ is the electronic density of states at the Fermi energy and $g^{\nu}_{\mathbf{k},\mathbf{k+q}}$ is the *electron-phonon matrix element*. This matrix element has already been introduced in an earlier equation however it has not been explicitly stated, namely in equation (24), and is

$$g^{\nu}_{n\mathbf{k},n'\mathbf{k+q}} = \langle n\mathbf{k}| \, \delta V^{\nu}_{\mathbf{q}} \, |n'\mathbf{k} + \mathbf{q}\rangle \, . \tag{35}$$

[22] The Eliashberg function can be split into different $n\mathbf{k}$-states, leaving

$$\alpha^2F_{n\mathbf{k}}(\omega) = \sum_{n'\mathbf{k+q},\nu} |g^{\nu}_{n\mathbf{k},n'\mathbf{k+q}}|^2 \delta(\varepsilon_{\mathbf{k}} - \varepsilon_{\mathbf{k+q}} - \hbar\omega^{\nu}_{\mathbf{q}})\delta(\omega - \omega^{\nu}_{\mathbf{q}}). \tag{36}$$

The EPC parameter $\lambda$ is related through [26]

$$\lambda_{n\mathbf{k}} = 2\int_0^{\infty} \frac{\mathrm{d}\omega}{\omega} \alpha^2F_{n\mathbf{k}}(\omega), \tag{37}$$

and the lifetime broadening by [22]

$$\Gamma_{\mathbf{k}} = 2\pi\hbar \int_0^{\infty} \mathrm{d}\omega \alpha^2F_{n\mathbf{k}}(\omega). \tag{38}$$

If the Eliashberg function consists of a single dominant frequency and a single dominant mode, the parameter $\lambda$ can be approximated to

$$\lambda \approx \frac{2}{\Omega} \int_0^\infty \mathrm{d}\omega \alpha^2 F_{n\mathbf{k}}(\omega) \tag{39}$$

where $\Omega$ is the dominant frequency of the mode. In this approximation there is a direct relationship between the lifetime broadening and the electron-phonon coupling constant $\lambda$, given by

$$\lambda_{n\mathbf{k}} \approx \frac{\Gamma_{n\mathbf{k}}}{\pi\hbar\Omega}. \tag{40}$$

which is quantitative measure of the electron-phonon coupling.

## 2.7 Superconductivity

The first person ever to describe superconductivity was Heike Kamerlingh Onnes in 1911[27]. His works were related to the liquefaction of helium and the conductivity of metals in low temperature. The first microscopic theory of superconductivity was presented much later, in 1957, called the Bardeen-Cooper-Schrieffer(BCS) theory. The theoretical framework for superconductivity consists of two areas. Firstly, a pairing formalism generating the superconductivity, and secondly, an attractive interaction between two electrons resulting in these pairs[26] called Cooper pairs. For this theory the trio received a nobel prize in physics 1972. As the scientific understanding of superconductivity went forward, a common interest of reaching higher temperature of superconductivity emerged. The BCS theory however cannot explain all superconductors, such as the high $T_c$ cuprates, and to this day, there is no united theory behind the high $T_c$ superconductors[28]. It should however be noted that BCS theory puts no upper limit on $T_c$, and that high $T_c$ superconductivity can be achieved by this theory; the highest recorded transition temperature explained by BCS theory is 203 K at high pressure[29].

Migdal and Eliashberg took the BCS theory and improved it, resulting in the Migdal-Eliashberg theory and the subsequent Eliashberg equations, thus creating a very accurate representation of almost all existing superconductors[26]. Part of the derivation of the set of equations can be found in Appendix B. Another physicist named McMillan simplified and solved these equations by fitting parameters to a set of data by using the spectral function for lead, resulting in an accurate formula for $\lambda < 2$ and $\mu^* < 0.15$, where $\lambda$ is the usual EPC-parameter and $\mu^*$ is the effective Coulomb repulsion[30],

$$\frac{1}{\mu^*} = \frac{1}{\mu} + \ln(\omega_{el}/\omega_{ph}) \tag{41}$$

where $\mu$ is the coulomb repulsion, $\omega_p h =$ is the high-frequency cutoff frequency in the Eliashberg function and $\omega_{el}$ is the plasma frequency. Usually, $\mu^*$ has a value of around 0.1 in s and p-band superconductors[1], and it will be the assumed value in this thesis. McMillan arrived at an expression for the transition temperature which was subsequently improved by P.B. Allen and R.C. Dynes arriving at the formula

$$T_c = \frac{\hbar\omega_{log}}{1.20} \exp\left[-\frac{1.04(1+\lambda)}{\lambda - \mu^*(1+0.62\lambda)}\right] \tag{42}$$

where $\omega_{log} \approx 725.9\,\mathrm{cm}^{-1}$ is the logarithmically averaged phonon frequency. The numerator in the prefactor corresponds to the temperature 1035.77 K[1].

# 3 Method

This chapter details the methods used for the tight-binding model with the nearest neighbour approximation. We cover how the transfer and overlap matrices are treated, as well as how the electronic band structure is calculated from the secular equation. It also describes the algorithms used for determining the lifetime broadening by means of numerical integration, and estimating the spectral function via the Kramer-Kronig transform.

## 3.1 Tight Binding Model of Graphene with Nearest Neighbour Approximation

In pure graphene both the A and B atoms in the unit cell are carbon atoms with identical atomic orbitals. Carbon has the electron configuration C: $1s^2 2s^2 2p^2$, where the $2s$ and $2p$ electrons are involved in the energy dispersion, as the inner most state $1s$ stays inert. Every unit cell of graphene contains two carbon atoms with $sp^2$ hybridization, and each atom contributes with four orbitals $2s$, $2p_x$, $2p_y$, and $2p_z$. Where the three first orbitals participate in $\sigma$ bonds and the later, $2p_z$, orbital contributes to the $\pi$ bond. Since there are two atoms $A, B$ in each unit cell, we have six orbitals contributing to $\sigma$-bands. We define the basis of local atomic orbitals $\phi_j$ according to Section 2.1.2:

$$\begin{aligned} |2s\rangle &= \frac{\zeta_{2s}^{5/2}}{\sqrt{96\pi}} r e^{-\zeta r/2}, \quad |2p_z\rangle = \frac{\zeta_{2p}^{5/2}}{\sqrt{32\pi}} x e^{-\zeta r/2} \\ |2p_x\rangle &= \frac{\zeta_{2p}^{5/2}}{\sqrt{16\pi}} x e^{-\zeta r/2}, \quad |2p_y\rangle = \frac{\zeta_{2p}^{5/2}}{\sqrt{16\pi}} y e^{-\zeta r/2} \end{aligned} \tag{43}$$

where $\zeta_{2s} = 5.7, \zeta_{2p} = 3.25$, given in Rydberg and $x, y, z, r$ are given in atomic units (Bohr radius).

The unit cell of graphene is depicted in Figure 8 together with the chosen coordinate system. The primitive lattice vectors are defined in Cartesian coordinates as

$$\mathbf{a}_1 = a\left(\frac{1}{2}, \frac{\sqrt{3}}{2}\right), \quad \mathbf{a}_2 = a\left(\frac{1}{2}, -\frac{\sqrt{3}}{2}\right). \tag{44}$$

where $a = 4.65\,\text{Å}$ is the lattice constant. The origin is taken to be in the middle of the unit cell which gives the following position vectors for the A and B sites

$$\mathbf{r}_A = a\left(-\frac{1}{2\sqrt{3}}, 0\right), \quad \mathbf{r}_B = a\left(\frac{1}{2\sqrt{3}}, 0\right). \tag{45}$$

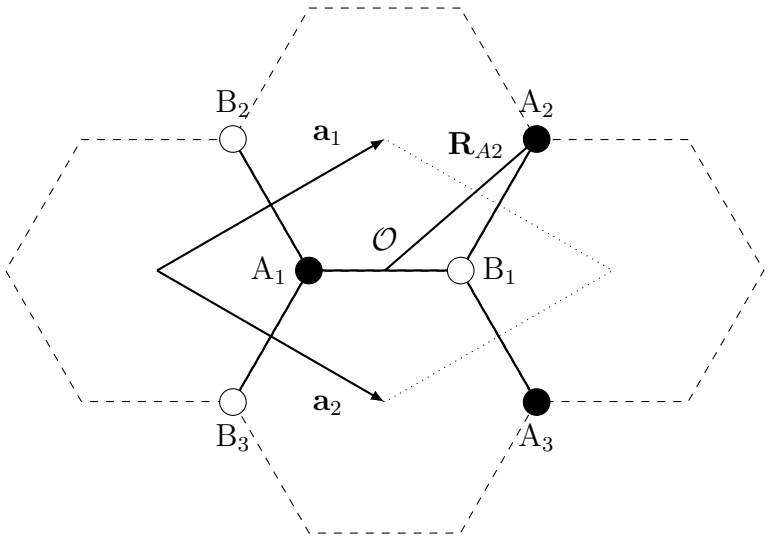


Figure 8: *Schematic figure of the unit cell with the atomic basis $A, B$ in the hexagonal graphene structure with only the nearest neighbours. The lattice vectors are denoted $\mathbf{a}_1, \mathbf{a}_2$.*

In the tight binding model, the single electron wavefunction consists of a sum of Bloch orbitals where the sum is taken over all unit cells of the crystal. However, since the atomic orbitals falls off exponentially fast it often a good approximation to limit the number of summed unit cells to only those nearest to the main unit cell. This is also true for graphene, where we can go one step further and use the *nearest neighbour approximation* (NNA). In NNA, atoms in the unit cell only interact with their nearest neighbour, this is depicted in Figure 8 where the $A$ atom only interacts with the three nearest $B$ atoms and vice versa. The relevant atomic positions are thus

$$\mathbf{R}_{A_1} = a\left(\frac{1}{\sqrt{3}}, 0\right) \qquad \mathbf{R}_{B_1} = a\left(\frac{1}{\sqrt{3}}, 0\right) \tag{46}$$

$$\mathbf{R}_{A_2} = a\left(\frac{1}{2\sqrt{3}}, \frac{1}{2}\right) \qquad \mathbf{R}_{B_2} = a\left(-\frac{1}{2\sqrt{3}}, \frac{1}{2}\right) \tag{47}$$

$$\mathbf{R}_{A_3} = a\left(-\frac{1}{2\sqrt{3}}, -\frac{1}{2}\right) \qquad \mathbf{R}_{B_3} = a\left(-\frac{1}{2\sqrt{3}}, -\frac{1}{2}\right) \tag{48}$$

The consequences of omitting the next-nearest neighbours is discussed in Section 5.2.1.

## 3.2 Transfer and Overlap Interactions in Graphene Orbitals

Recall the matrices $H$ and $S$, which denote the transfer matrix and the overlap matrix respectively. Their elements are written

$$\begin{aligned} H_{ij} &= \langle \Phi_i | \, \hat{H} \, | \Phi_j \rangle = \frac{1}{N} \sum_{\mathbf{R}_A} \sum_{\mathbf{R}_B} e^{i\mathbf{k}\cdot(\mathbf{R}_A - \mathbf{R}_B)} \, \langle \phi_i(\mathbf{r} - \mathbf{R}_A) | \, \hat{H} \, | \phi_j(\mathbf{r} - \mathbf{R}_B) \rangle \\ S_{ij} &= \langle \Phi_i | \Phi_j \rangle = \frac{1}{N} \sum_{\mathbf{R}_A} \sum_{\mathbf{R}_B} \langle \phi_i(\mathbf{r} - \mathbf{R}_A) | \phi_j(\mathbf{r} - \mathbf{R}_B) \rangle \end{aligned} \tag{49}$$

where $\phi$ denotes atomic orbitals. The $H_{ij}$ matrix elements can be described to characterise the transition of an electron from an initial orbital state $j$ to a final state $i$, whilst the $S_{ij}$ elements describe the physical overlap of the orbitals. However, this interpretation is not compatible for $i = j$, in which case the most convenient interpretation is an expectation value of the energy in that particular state.

Given the four orbitals $2s, 2p_x, 2p_y, 2p_z$, the transfer matrix $H$ will be an $8 \times 8$ size matrix[15]:

$$H = \begin{array}{c} \begin{array}{cccccccc} 2s^A & 2p_x^A & 2p_y^A & 2s^B & 2p_x^B & 2p_y^B & 2p_z^A & 2p_z^B \end{array} \\ \begin{pmatrix} . & \cdots & \cdots & \cdots & \cdots & . & & \\ \vdots & \ddots & & & & \vdots & & \\ \vdots & & H_\sigma & & & \vdots & & \\ \vdots & & & \ddots & & \vdots & & \\ \vdots & & & & \ddots & \vdots & & \\ . & \cdots & \cdots & \cdots & \cdots & . & & \\ & & & & & & H_\pi & \cdots \\ & & & & & & \vdots & \ddots \end{pmatrix} \end{array} \begin{array}{c} 2s^A \\ 2p_x^A \\ 2p_y^A \\ 2s^B \\ 2p_x^B \\ 2p_y^B \\ 2p_z^A \\ 2p_z^B \end{array} \tag{50}$$

where all elements $\langle 2p_z | \, \hat{H} \, | \phi_j \rangle$, $\phi_j \neq 2p_z$ are zero due to the orthogonality detailed in Section 2.1.2. We define the two matrices $H_\sigma \, (6 \times 6)$ and $H_\pi \, (2 \times 2)$.

We now wish to calculate the elements in detail, and introduce the *hopping parameters* $H$ of the transfer matrix, which are calculated from experimental data. The "hopping" of an electron from an orbital on atom $B$ to $A$ may be written

$$\begin{aligned} H_{ss\sigma} &= \left\langle 2s^A \right| \hat{H} \left| 2s^B \right\rangle \\ H_{sp\sigma} &= \left\langle 2s^A \right| \hat{H} \left| 2p_\parallel^B \right\rangle \\ H_{pp\sigma} &= \left\langle 2p_\parallel^A \right| \hat{H} \left| 2p_\parallel^B \right\rangle \\ H_{pp\pi} &= \left\langle 2p_\perp^A \right| \hat{H} \left| 2p_\perp^B \right\rangle \end{aligned} \tag{51}$$

but on identical atoms we get the expectation values

$$\begin{aligned}\varepsilon_{2s} &= \left\langle 2s^A \right| \hat{H} \left| 2s^A \right\rangle = \left\langle 2s^B \right| \hat{H} \left| 2s^B \right\rangle \\ \varepsilon_{2p} &= \left\langle 2p^A \right| \hat{H} \left| 2p^A \right\rangle = \left\langle 2p^B \right| \hat{H} \left| 2p^B \right\rangle\end{aligned} \tag{52}$$

Taking only the nearest neighbours in regard, the choice of hopping parameters stem from the possible projections of the $p$ and $s$ orbitals on the binding axis, and $\parallel, \perp$ indicate the parallel and perpendicular components respectively. The $s$ orbitals are spherically symmetrical around a binding axis and thus not relevant to much analysis.[15][13]

Consider for example an $s$ and $p$ orbital along a binding axis, see Figure 9. The $p$ orbital may be decomposed as

$$|2p\rangle = \cos\theta \left| 2p_\parallel \right\rangle + \sin\theta \left| 2p_\perp \right\rangle, \tag{53}$$

We can thus determine the hopping integral as

$$\begin{aligned}\langle 2s| \hat{H} |2p_x\rangle &= \langle 2s| \hat{H} \left( \cos\theta \left| 2p_\parallel \right\rangle + \sin\theta \left| 2p_\perp \right\rangle \right) \\ &= \cos\theta \langle 2s| \hat{H} \left| 2p_\parallel \right\rangle = H_{sp\sigma} \cos\theta\end{aligned} \tag{54}$$

using the intrinsic orthogonality conditions detailed in Section 2.1.2. Take next two arbitrary $p$ orbitals $|2p\rangle, |2p'\rangle$ in the same fashion, with two angles $\theta, \theta'$ to the binding axis

$$\begin{aligned}\langle 2p| \hat{H} |2p'\rangle =& \left\langle 2p_\parallel \right| \hat{H} \left| 2p'_\parallel \right\rangle \cos\theta\cos\theta' + \langle 2p_\perp| \hat{H} |2p'_\perp\rangle \sin\theta\sin\theta' \\ =& H_{pp\sigma} \cos\theta\cos\theta' + H_{pp\pi} \sin\theta\sin\theta'\end{aligned} \tag{55}$$

In the hexagonal graphene, only three modulus angles are possible: $|\theta| = \pi/6, \pi/3, \pi$.

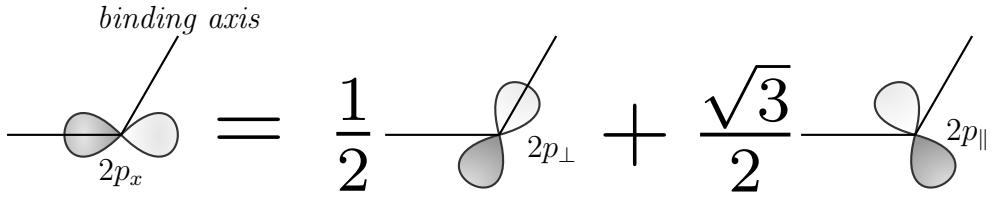


Figure 9: *Grahical representation of the orbital decomposition along a binding axis, specifically of element $H_{12}$ of the transfer matrix.*

Consider now Figure 9, which displays $H_{12}$, a total hopping matrix element. Using our previous calculations we conclude

$$\begin{aligned} H_{12} =& \frac{1}{N} \sum_{\mathbf{R}_A} \sum_{\mathbf{R}_B} e^{i\mathbf{k}\cdot(\mathbf{R}_A - \mathbf{R}_B)} \left\langle 2s^A(\mathbf{r} - \mathbf{R}_A) \right| \hat{H} \left| 2p_x^B(\mathbf{r} - \mathbf{R}_B) \right\rangle \\ =& \sum_{\mathbf{R}_B} e^{i\mathbf{k}\cdot\mathbf{R}_B} \left\langle 2s^A(\mathbf{r}) \right| \hat{H} \left| 2p_x^B(\mathbf{r} - \mathbf{R}_B) \right\rangle \\ =& H_{sp\sigma} \sum_{\mathbf{R}_B} e^{i\mathbf{k}\cdot\mathbf{R}_B} \cos\theta_{\mathbf{R}_B} \\ =& H_{sp\sigma} \left( -e^{iak_x/\sqrt{3}} + \frac{1}{2} e^{ia(-k_x/2\sqrt{3} + k_y/2)} + \frac{1}{2} e^{ia(-k_x/2\sqrt{3} - k_y/2)} \right), \end{aligned} \tag{56}$$

the other elements are calculated in the same manner.

When it comes to the overlap elements $S_{ij}$, we introduce an important approximation called the *orthogonal basis*, which differs to the previous analysis of $H_{ij}$ in that atomic orbitals on different atoms have no overlap, and that different atomic orbitals are entirely orthonormal, such that $S$ will be the unit matrix: [15]

$$S_{ij} = \begin{cases} 1, & i = j \\ 0, & i \neq j \end{cases} \tag{57}$$

The impact of this approximation is discussed in Section 5.2.2. The tight binding parameters in equation (51) and (52) are chosen to agree with DFT calculations [31]. The values used in this thesis are

$$\begin{array}{ll} H_{ss\sigma} = -6.769\,\text{eV} & H_{sp\sigma} = 5.58\,\text{eV} \\ H_{pp\sigma} = 4.537\,\text{eV} & H_{pp\pi} = -2.033\,\text{eV} \\ \varepsilon_{2s} = -8.868\,\text{eV} & \varepsilon_{2p} = 0\,\text{eV}. \end{array} \tag{58}$$

## 3.3 Electronic $\sigma$ and $\pi$-band Calculation with TB

With the use of the secular equation (15) we get a $6 \times 6$ transfer matrix $H_\sigma$. This matrix can be divided into four smaller separate $3 \times 3$ matrices,

$$H_\sigma = \begin{pmatrix} H_{AA} & H_{AB} \\ H_{BA} & H_{BB} \end{pmatrix}, \tag{59}$$

where $AA$ and $AB$ marks the integrals between orbitals from atom to atom in the unit cell. In the case of graphene where atom $A$ and $B$ are the same, by

symmetry, conclude that matrices $H_{AA}$ and $H_{BB}$ are identically equal, For the diagonal elements in $H_\sigma$ we have thus

$$H_{BB} = H_{AA} = \frac{1}{N} \sum_{\mathbf{R}_A = \mathbf{R}_{A'}}^{N} \langle \phi(\mathbf{r} - \mathbf{R}_A) | \hat{H} | \phi(\mathbf{r} - \mathbf{R}_A) \rangle \tag{60}$$

This is equivalent to a matrix of the expectation value hopping parameters in Section 3.2. We thus conclude that due to the orthogonality conditions of the atomic orbitals, the $H_{AA}$ matrix will be entirely diagonal, with the elements

$$\begin{aligned} H_{AA} = H_{BB} &= \begin{pmatrix} \langle 2s^A | \hat{H} | 2s^A \rangle & 0 & 0 \\ 0 & \langle 2p_x^A | \hat{H} | 2p_x^A \rangle & 0 \\ 0 & 0 & \langle 2p_y^A | \hat{H} | 2p_y^A \rangle \end{pmatrix} \\ &= \begin{pmatrix} \varepsilon_{2s} & 0 & 0 \\ 0 & \varepsilon_{2p} & 0 \\ 0 & 0 & \varepsilon_{2p} \end{pmatrix} \end{aligned} \tag{61}$$

and the off diagonal elements are zero.

For the mixed-atom matrices $H_{AB}, H_{BA}$ we arrive at a similar expression, namely

$$H_{BA} = H_{AB}^\dagger = \frac{1}{N} \sum_{\mathbf{R}_A}^{N} \sum_{\mathbf{R}_B} e^{i\mathbf{k}\cdot(\mathbf{R}_B - \mathbf{R}_A)} \langle \phi(\mathbf{r} - \mathbf{R}_A) | \hat{H} | \phi(\mathbf{r} - \mathbf{R}_B) \rangle^\dagger , \tag{62}$$

where $^\dagger$ denotes the Hermitian transpose. The components of these matrices will be mixed in both orbital and atoms, and thus not diagonal, like in the previous case. Rather, we use the component separation method detailed in Section 3.2:

$$H_{AB} = H_{BA}^\dagger = \begin{pmatrix} \langle 2s^A | \hat{H} | 2s^B \rangle & \langle 2p_x^A | \hat{H} | 2s^B \rangle & \langle 2p_y^A | \hat{H} | 2s^B \rangle \\ \langle 2s^A | \hat{H} | 2p_x^B \rangle & \langle 2p_x^A | \hat{H} | 2p_x^B \rangle & \langle 2p_y^A | \hat{H} | 2p_x^B \rangle \\ \langle 2s^A | \hat{H} | 2p_y^B \rangle & \langle 2p_x^A | \hat{H} | 2p_y^B \rangle & \langle 2p_y^A | \hat{H} | 2p_y^B \rangle \end{pmatrix} \tag{63}$$

The elements of this matrix are detailed in Appendix A.

In Section 3.2 it is argued that the overlap is equal to the identity matrix, $I$. With this approximation the $\sigma$-bands are calculated by determining the eigenvalues of the transfer matrix $H_\sigma$. The secular equation becomes

$$\det (H_\sigma - \varepsilon_{\mathbf{k}} I) = 0. \tag{64}$$

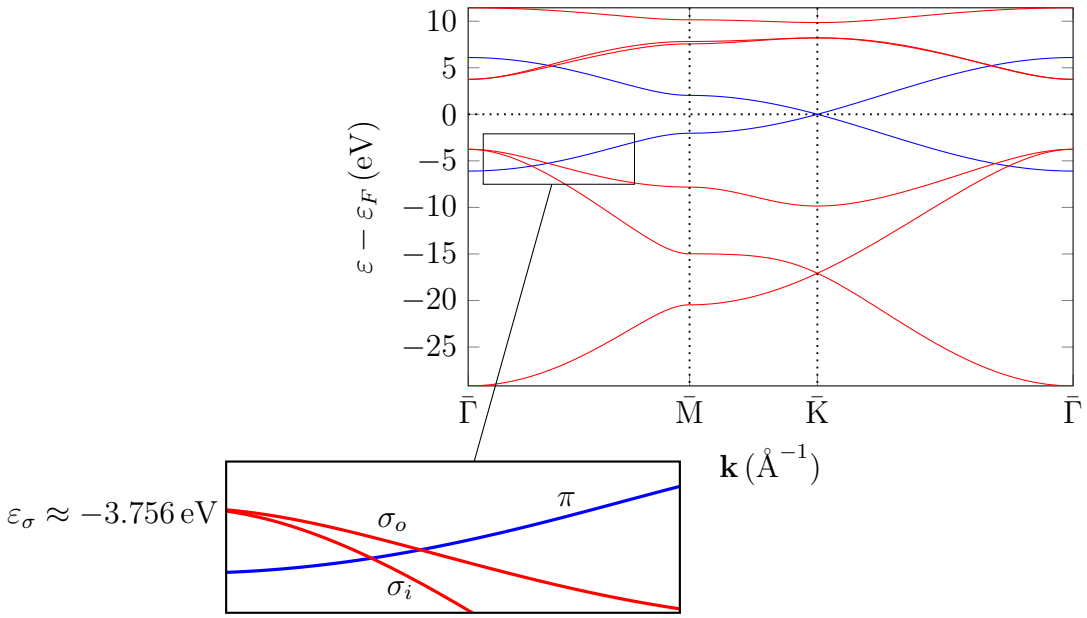


Figure 10: *The $\pi$ (blue) and $\sigma$ (red) electron bands of graphene calculated with a tight binding method, excluding next-nearest neighbours and any overlap between orbitals on different atoms. The lower $\pi$-band and the so called inner and outer $\sigma$-bands denoted $\sigma_i, \sigma_o$ are of certain interest.*

The solution bandstructure is presented in Figure 10.

As previously mentioned only the $2p_z$ orbitals contribute to the $\pi$-bands. Using the secular equation (15) again we define a $2\times2$ transfer matrix, in the same fashion as above. The matrix obviously follows the same symmetry rules as $H_\pi$

$$H_\pi = \begin{pmatrix} H_{AA}\ H_{AB} \\ \\ H_{BA}\ H_{BB} \end{pmatrix}. \tag{65}$$

In component form we get that

$$\begin{aligned} H_{AA} &= \left\langle 2p_z^A \right| \hat{H} \left| 2p_z^B \right\rangle \\ &= \frac{1}{N} \sum_{\mathbf{R}_A = \mathbf{R}_{A'}}^{N} \left\langle 2p_z(\mathbf{r} - \mathbf{R}_A) \right| \hat{H} \left| 2p_z(\mathbf{r} - \mathbf{R}_A) \right\rangle = \epsilon_{2p}. \\ H_{AB} &= \left\langle 2p_z^A \right| \hat{H} \left| 2p_z^B \right\rangle \\ &= \sum_{i=1}^{3} H_{pp\pi} e^{i\mathbf{k}\cdot\mathbf{R}_{Ai}}, \end{aligned} \tag{66}$$

analogous to the calculations of the $\sigma$-bands. Element $H_{BA}$ is given by the complex conjugate of $H_{AB}$, and $H_{BB}$ is obtained by the fact that $H_{AA} = H_{BB}$. The eigenvalues are yet again given by the secular equation, such that

$$\det\left(H_\pi - \varepsilon_{\mathbf{k}} I\right) = 0. \tag{67}$$

The diagonalisation in turn for $\pi$ and $\sigma$ is implemented numerically in FORTRAN, using the `ZHPEVD` subroutine in LAPACK.

The solution to the band structure as derived numerically through the tight-binding model and secular equation is presented in Figure 10. We define the important $\sigma_i, \sigma_o, \pi$-bands, at the top of the band structure close to the Fermi energy, and thus equivalent to the valence bands.

The contribution of these bands to the EPC is non-negligible, and we will consider especially photo-holes excited in the $\sigma_o$-band.

## 3.4 Numerical Estimate of the Lifetime Broadening

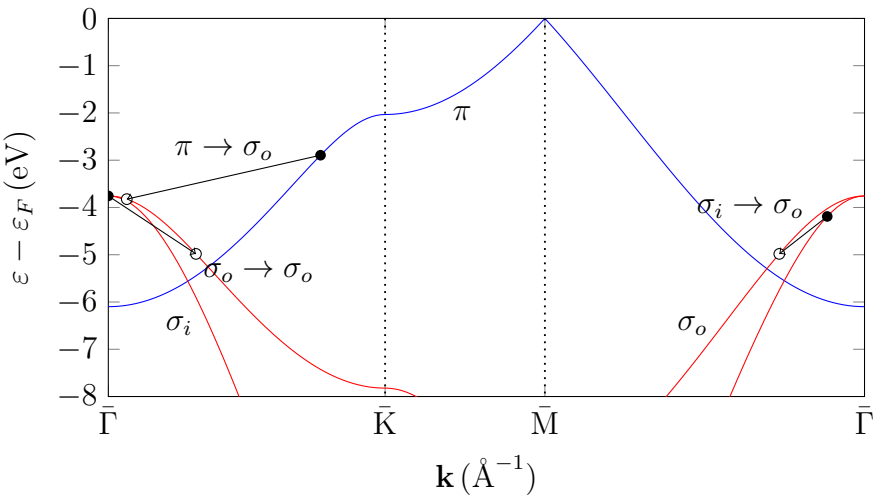


Figure 11: *The top of the graphene $\pi$- and $\sigma$-bands as calculated in this thesis, with sample hopping. The hopping between bands denoted as $\sigma_i, \sigma_o$ and $\pi$ are of special interest in the EPC due to their proximity to the Fermi energy $\varepsilon_F$.*

According to equation (24) in Section 2 the relevant contribution of the phonon to the lifetime broadening $\Gamma_n$ is described by the hopping matrix element

$$\langle n\mathbf{k}|\, \delta V_{\nu\mathbf{q}}\, |n'\mathbf{k}+\mathbf{q}\rangle = \frac{1}{N}\sum_{sj}\sum_{s'j'} c^*_{nsj} c_{n's'j'} \sum_{\mathbf{R},\mathbf{R}',\mathbf{R}''} H' e^{i\mathbf{k}\cdot\mathbf{R}} e^{i\mathbf{q}\cdot\mathbf{R}''} e^{i(\mathbf{k}+\mathbf{q})\cdot\mathbf{R}'} \tag{68}$$

where $\mathbf{R} = \mathbf{R}(s), \mathbf{R}' = \mathbf{R}(s'), \mathbf{R}'' = \mathbf{R}(s'')$, and

$$H' = \langle \phi_j(\mathbf{r} - \mathbf{R}(s)) | \, \delta V_\nu \, | \phi_{j'}(\mathbf{r} - \mathbf{R}(s')) \rangle \tag{69}$$

is the hopping induced by the potential perturbation $\delta V_\nu$ in the basis orbitals, which we are forced to solve for numerically in real space.

The integration algorithm is simple numerical Riemann integration. That is, we first model the unit cell as a rectangle in real space, with partitioning into small rectangles with dimensions $\Delta x, \Delta y, \Delta z$. As such, the hopping integral $H'$ over the neareast neighbours is

$$\begin{aligned} H' = \langle \phi_j(\mathbf{r} - \mathbf{R}(s)) | \, \delta V_\nu \, | \phi_{j'}(\mathbf{r} - \mathbf{R}(s')) \rangle &= \int \phi_j^* \delta V_\nu \phi_{j'} \, \mathrm{d}r \\ &= \sum_{\Delta x, \Delta y, \Delta z} \phi_j^* \delta V_\nu \phi_{j'} \, \Delta x \Delta y \Delta z. \end{aligned} \tag{70}$$

The integral over real space by means of rectangular sections has apparent numerical overlap, however, and the contribution from the unit cell is obtained by subtracting these overlaps, see Figure 12.

In addition to the hopping matrix element, a delta function is needed to ensure energy conservation. The delta function is modeled numerically as a Lorentzian function with a small width.

### 3.4.1 Deformation Potential and Atomic Displacement

Because phonons introduce a displacement of the ions in the lattice, the potential field will move with the displacement, giving rise to the distortion $\delta V$ to the potential $V$ necessary to compute the hopping matrix element equation (69). Given that the displacement is small compared to the distance between neighbouring atoms, the potential distortion does not have an effect on the local potential at neighbouring atoms. This approximation is called the *rigid ion approximation* (RIA).

The potential is thus considered to move rigidly with the displacement of the atom (as the displacement has a greater influence over the local field than any field from neighbouring atoms). We model phonon vibrations as harmonic oscillators, with a deformation potential on the Gaussian form

$$V(\mathbf{r}) = -V_0 e^{-(r/\alpha)^2} \tag{71}$$

The choice of potential has the benefit of a series expansion to the first order such that

$$V_0 e^{-(r/\alpha)^2} \approx V_0 \left(1 - \frac{r^2}{\alpha^2}\right), \tag{72}$$

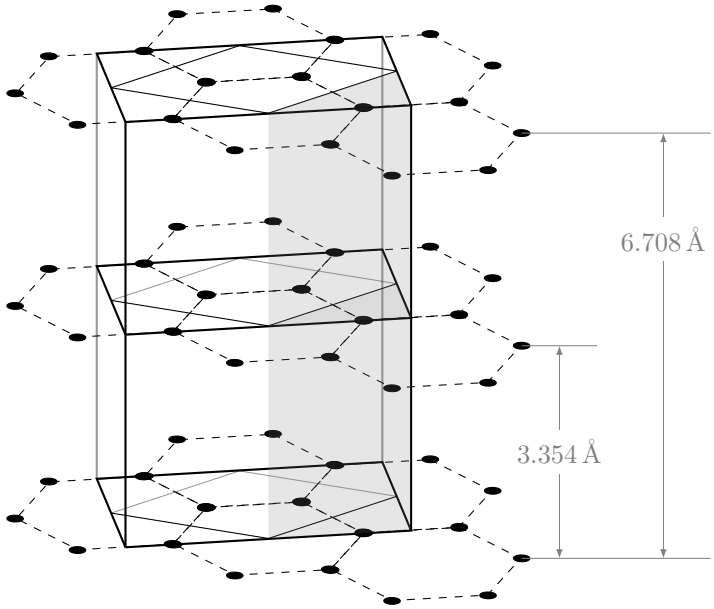


Figure 12: *The unit cell in a graphene layer and schematic integration of the phonon potential matrix element, where the shaded volume denotes the overlap between the rectangular integration areas. Graphene is a purely 2D material, and as such we consider only one layer.*

and thus behaves like a harmonic potential for small $\mathbf{r}$, but vanishes at great distances. $V_0$ is the potential strength, and $\alpha$ is the screening parameter that determines how localised the potential is i.e. the variance of the potential. Both parameters have been fitted to experiment, with reported values $\alpha = 1.5\,\text{a.u.}$, $V_0 = 90\,\text{eV}$.

Now consider the perturbation potential due to the displacement $\mathbf{Q}_\nu$ of an atom by a phonon mode $\nu$, the distortion to the first order of approximation will be

$$\begin{aligned}\delta V_\nu(\mathbf{r}) =& -\nabla V \cdot \mathbf{Q}_\nu \\ =& \frac{2V_0}{\alpha^2} e^{-(r/\alpha)^2} \mathbf{r} \cdot \mathbf{Q}_\nu,\end{aligned} \tag{73}$$

in line with the RIA. We approximate the displacement $Q_\nu$ as the mean square displacement in a harmonic oscillator, where the displacement from the ground state to the first excited state is

$$\left|\langle 0|\, Q_\nu \,|1\rangle\right|^2 = \frac{\hbar}{2m\omega_{\nu\mathbf{q}}} \equiv Q_\nu^2 \tag{74}$$

where $\omega_{\nu\mathbf{q}} = \Omega_{\nu\mathbf{q}}$ is the phonon frequency dispersion and $m$ is the ion mass.

## 3.5 Calculation of the Numerical Spectral Function

Now given numerical expressions for $\delta V$ and subsequently $\Gamma$, using the theoretical identity

$$\operatorname{Im}\Sigma = \frac{1}{2}\Gamma,$$

we may estimate the measured spectral function.

We arrive at the real part of the self energy $\Sigma$ by means of the Kramers-Kronig relations in equation (33). The real part may thus be written

$$\text{Re }\Sigma(\varepsilon) = \frac{1}{2\pi}\mathcal{P}\int_{-\infty}^{\infty}\frac{\Gamma_n}{\varepsilon' - \varepsilon}d\varepsilon' \tag{75}$$

The non-convergence of this integral presents some difficulties in its numerical calculation. We therefore utilise the convolution theorem in $\varepsilon$

$$\text{Re }\Sigma(\varepsilon) = \frac{1}{2}\left(\frac{1}{\varepsilon} * \Gamma_n(\varepsilon)\right) = \text{Re }\Sigma(\varepsilon) = \frac{1}{2}\mathcal{F}^{-1}\left(\mathcal{F}\left(\frac{1}{\varepsilon}\right)\cdot\mathcal{F}\left(\Gamma_n\right)(\varepsilon')\right), \tag{76}$$

where $*$ denotes the convolution, and $\mathcal{F}$ marks the Fourier transform. This algorithm is aptly implemented in the MATLAB Hilbert transform `hilbert`. The function applies to our problem since equation (75) is equivalent to

$$\text{Re }\Sigma(\varepsilon) = -\frac{1}{2}\,\text{Im }\mathcal{H}(\Gamma_n)(\varepsilon) \tag{77}$$

where $\mathcal{H}$ marks the Hilbert transform. The MATLAB function reportedly transforms nice functions within rounding-off error.

The spectral function as defined in equation (29) is a lorentzian in $\varepsilon$ and $\mathbf{k}$. However, we approximate the $\mathbf{k}$ dependence as small, and on the band energy $\varepsilon_{n\mathbf{k}}$ the energy-wavevector is a bijection: This means we may neglect the $\mathbf{k}$ dependence and instead only consider the spectral function with respect to the energy and band energy.[32]

The spectral function is a Lorentzian with a maximum at

$$\varepsilon = \varepsilon_n + \text{Re }\Sigma(\varepsilon),$$

where we try to solve for $\varepsilon$. However, in a first order approximation we take $\varepsilon = \varepsilon_i$ as a constant scanning parameter. We then choose to scan over $\varepsilon_{n\mathbf{k}}$, such that for each $i, \mathbf{k}$

$$A_n(\varepsilon_i, \mathbf{k}) = \frac{1}{\pi}\frac{\operatorname{Im}\Sigma_n(\varepsilon_i)}{\left(\varepsilon_i - \varepsilon_{n\mathbf{k}} - \operatorname{Re}\Sigma_n(\varepsilon_i)\right)^2 + \left(\operatorname{Im}\Sigma_n(\varepsilon_i)\right)^2}. \tag{78}$$

In order to determine the spectral function and especially the real part of the self energy we need to make a few assumptions [32]. The band structure for the

anti-binding $\sigma_o$-band, see Figure 10, is not normally accessible for analysis in the spectral function. However, we will assume a hole-particle symmetry in order to symmetrise the imaginary part of the self energy $\Gamma_{n\mathbf{k}}$ for the Fourier transform. In practice, this means the resulting lifetime broadening is mirrored in the Fermi energy $\varepsilon_F$.

Finally, we require that the continuation of the bands from $\bar{\Gamma}$-$\bar{\mathrm{K}}$ -$\bar{\mathrm{M}}$-$\bar{\Gamma}$ of lower energy has no significance on the real part of the self energy Re $\Sigma$ in our chosen energy window $\varepsilon_{n\mathbf{k}}$.

# 4 Results

The strength of the electron-phonon coupling in graphene is here quantified in terms of the lifetime broadening $\Gamma_{n\mathbf{k}}$ and the related coupling parameter $\lambda_{n\mathbf{k}}$. Putting these in relation to other research, the results include values of the transition temperature to superconductivity, according to McMillan's formula. The lifetime broadening is a measure of the transition rate of electrons at certain energies, and it exerts a change on the band structure of graphene visible in experiments such as ARPES. This renormalised band structure is here computed in terms of the spectral function.

## 4.1 The EPC: Lifetime Broadening and Spectral Function

The lifetime broadening quantifies the EPC in $\bar{\Gamma}$-$\bar{\mathrm{K}}$, see Figure 13a. We observe a sizeable step in $\Gamma_{n\mathbf{k}}$ that arises at approximately $-0.2\,\mathrm{eV}$ relative to the top of the $\sigma_o$ band. At approximately $-0.18\,\mathrm{eV}$, transition rate increases from nigh-zero to about $0.3\,\mathrm{eV}$, at which point $10\,\%$ of the broadening is due to $\Gamma_{po}$, and about $90\,\%$ due to $\Gamma_{io}, \Gamma_{oo}$. This indicates that the contribution of interband scattering is fairly high. Extrapolating from this, we may calculate the coupling strength in terms of the parameter $\lambda_{n\mathbf{k}}$. According to the approximative expression equation (40), the coupling strength is a mere scaling of the lifetime broadening, granted we have a single major contributing phonon frequency. Figure 13a indicates that this is the case around $0.2\,\mathrm{eV}$, which gives us a coupling strength of around $\lambda \approx 0.6$ at the kink.

Given values for both $\Gamma_{n\mathbf{k}}$ and Re $\Sigma$ we may graphically represent our results as the spectral function. Figure 14a is divided in the unperturbed band structure and the electron-phonon coupling in the $\sigma_o$ band, as defined in previous sections.

Consider the numerically estimated spectral function in Figure 14a and compare with the analytical expression

$$A_n(\varepsilon, \mathbf{k}) = \frac{1}{2\pi} \frac{\Gamma_n(\varepsilon, \mathbf{k})}{(\varepsilon - \varepsilon_n(\mathbf{k}) - \operatorname{Re}\Sigma_n(\varepsilon, \mathbf{k}))^2 + (\frac{1}{2}\Gamma_n(\varepsilon, \mathbf{k}))^2}.$$

The spectral function is a Lorentzian for every $\mathbf{k}$, and its width is determined by the aptly named lifetime broadening $\Gamma_{n\mathbf{k}}$, see Figure 13a. The shift from the unperturbed band is not miniscule, and calculated from

$$\varepsilon = \varepsilon_n(\mathbf{k}) + \operatorname{Re}\Sigma_n(\varepsilon, \mathbf{k}).$$

Evaluating the real part of the self-energy, we find that Re $\Sigma_n$ has a smooth, near constant shift, but a distinctive *kink* at the energy $-0.1759\,\mathrm{eV}$, see Figure 13a. This result is recurrent in the spectral function.

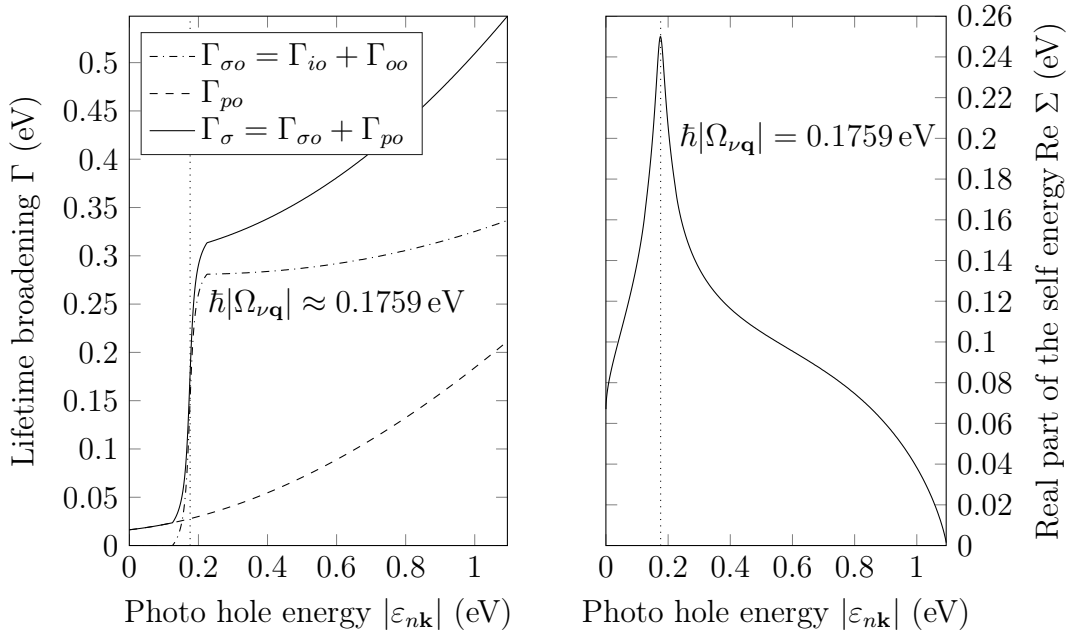


(a) *The lifetime broadening* $\Gamma_{n\mathbf{k}}$ *or equivalently the imaginary part of the self energy* Im $\Sigma$. *The lifetime broadening is near zero before* $\varepsilon \approx 0.2\,\mathrm{eV} \approx \hbar\Omega_{\nu\mathbf{q}}$. *It is noteworthy that the contribution of* $\pi$-$\sigma$ *interband hopping is sizeable for small energies.*

(b) *The real part of the self energy* Re $\Sigma$. *The real and imaginary parts are related via the Kramer-Kronig relations, and* Im $\Sigma = {}^1\!/_2\Gamma$. *The self energy constitutes a shift in the band structure due to the EPC, according the the spectral function* $A_{n\mathbf{k}}$.

Figure 13: *The numerically calculated real (b) and imaginary (a) parts of the self energy* $\Sigma = \mathrm{Re}\,\Sigma + i\,\mathrm{Im}\,\Sigma$, Im $\Sigma = {}^1\!/_2\Gamma_{n\mathbf{k}}$. *We require that the self energy is causal, and thus follows the Kramer-Kronig relations, connecting its complex parts.*

## 4.2 Transition Temperature $T_c$ from the Calculated $\lambda$-value

With given values of $\lambda$ calculated from the lifetime broadening, the $T_c$ can easily be obtained by the use of the equation (42), earlier discussed in the section of superconductivity. Values used in the equation are the effective Coulomb repulsion $\mu^* = 0.1$[33] and $\hbar\omega_{log} = 90.0\,\mathrm{meV}$ which is the logarithmic average phonon frequency[34]. From the numerical calculation a value of $\lambda$ is found to be around 0.6 at the kink. This yields a value of $T_c = 23.2\,\mathrm{K}$, see Figure 15

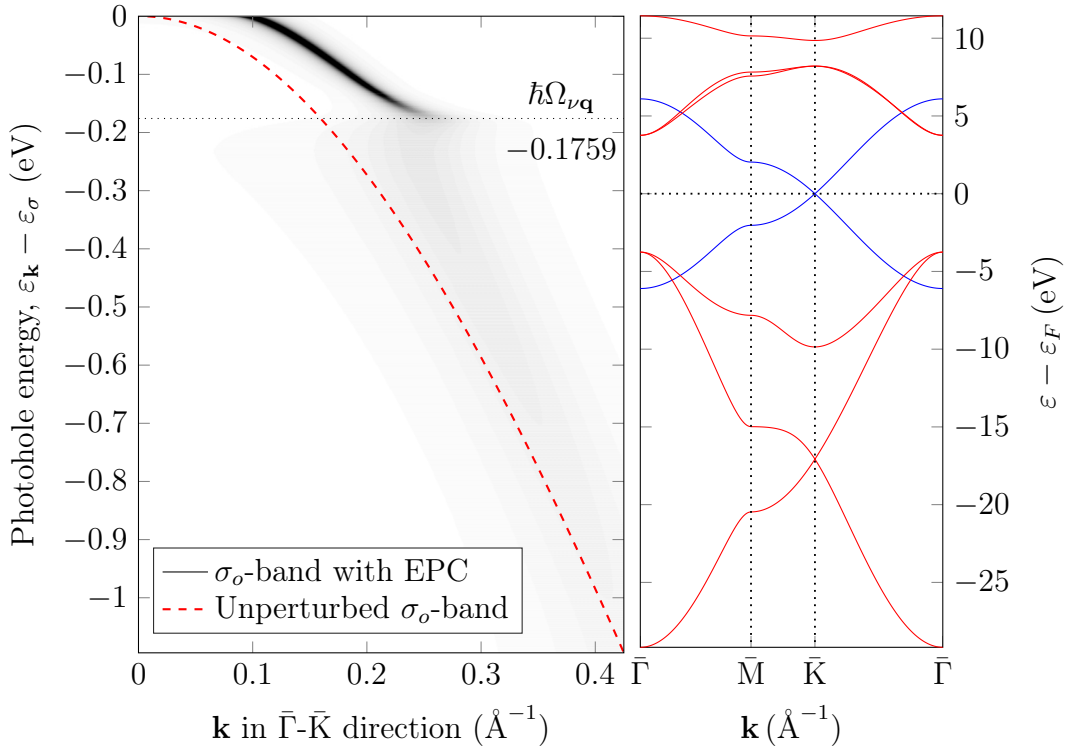


(a) *Resulting spectral function* $A_n(\varepsilon, \mathbf{k})$, *from the numerically estimated lifetime broadening* $\Gamma_{n\mathbf{k}}$ *due to electron-phonon coupling in graphene. Compare with the unperturbed bandstructure (red, dashed). There is a clear broadening and a small shift visible at* $\varepsilon \approx 0.2\,\mathrm{eV} \approx \hbar\Omega_{\nu\mathbf{q}}$.

(b) *The band structure of graphene calculated by means of the tight-binding method, relative to the Fermi energy* $\varepsilon_F$. *The* $\sigma$*-bands are coloured red and the* $\pi$*-bands are blue. Observe the three bands in below* $\varepsilon_F$, *the bands considered for the electron-phonon coupling in this paper.*

Figure 14: *The numerically calculated band structure of graphene in (b) and the perturbed* $\sigma_o$*-band due to electron-phonon coupling (a).*

# 5 Analysis and Discussion

In this following chapter the results are analysed and discussed, as well as potential sources of errors of all the approximations and calculations done. The transition temperature is discussed and compared to recent research. The possibility of superconductivity is also mentioned and the way of alter graphene through doping. Calculations are also done to check the reliability of the numerical calculations such as the condition number of the $H$-matrix and the residual for the $\Gamma$ calculations, to get an idea of the errors that might occur.

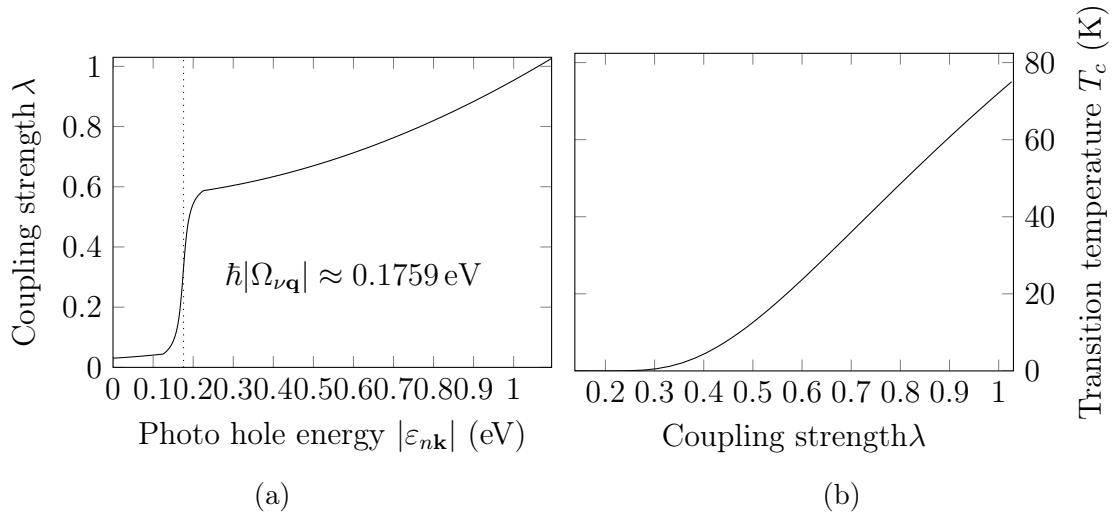


Figure 15: (a) *The calculated coupling strength $\lambda$ dependent on the photo hole energy.* (b) *McMillan's formula for $T_c$ as a function of $\lambda$ in the interval from* 0.2 *to* 1 *with* $\mu^* = 0.1$.

## 5.1 Analysis of the Results

### 5.1.1 The Spectral Function and ARPES Data

The background of our work is the investigation of the apparent kink in the $\sigma_o$-band, documented in the ARPES experiments on graphene, see Figure 7 in Section 2.5.1. Previous material has attempted to explain the kink by means of sublattice interference due to the cell structure of the material. The other main approach was through DFT calculations, which indicated that electron-phonon coupling might be to blame. Our results are based on a TB model, evaluating the lifetime broadening on the band.

The broadening $\Gamma_{n\mathbf{k}}$ has a distinctive increasing step at $-0.176\,\mathrm{eV}$, approximately the value given of the constant phonon dispersion $\omega_{\nu\mathbf{k}} = \Omega_{\nu\mathbf{k}} = -0.175\,\mathrm{eV}$. This induces a similar peak in the real part of the self energy at the same energy, which is realised as a kink in our spectral function. This result appears to correspond qualitatively to that of the ARPES experiment, compare Figure 14a and Figure 7.

We collect the data of the band structure, ARPES and the spectral function in Figure 16, where we have a strong correspondence with the experimental data. There are a few aberrations, however; the spectral function is slightly more shifted than the ARPES data. The shift is due to Re $\Sigma$, which was calculated by means of FFT in the Kramer-Kronig-transform. FFTs are in general poor at replicating a correct amplitude, and depend on the number of data points and periodicity of

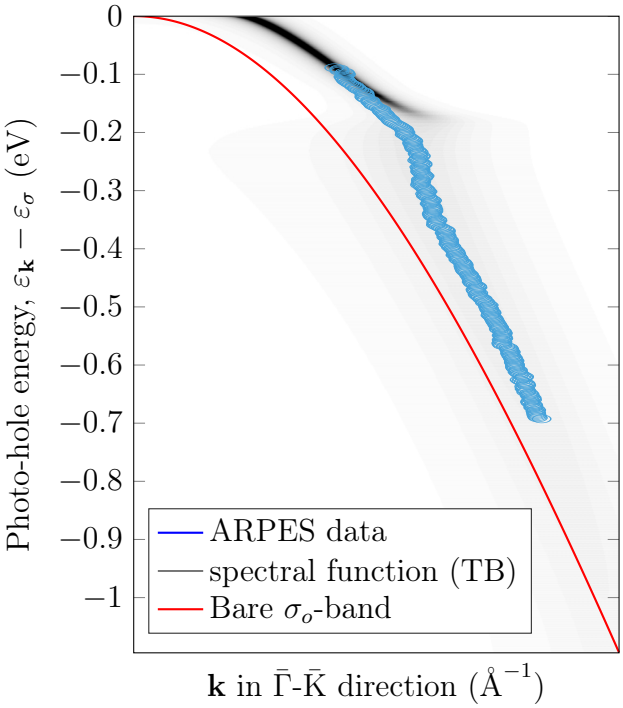


Figure 16: *Comparison of the ARPES experimental data of the electron distribution in the top $\sigma$-band, the simulated spectral function due to EPC, and the unperturbed band. The so called kink is clearly visible at around $-0.2\,\mathrm{eV}$, relative to the top of the band. The ARPES data was taken from [1] with the permission of the authors.*

the data. Our method introduced a periodicity in the particle-hole symmetry, but possibly more sophisticated methods must be employed.

What is surprising about our model however, is the significant value of the interband scattering $\pi \to \sigma_o$, see Figure 13a. This is unexpected, but previous authors have suspected this behaviour[1].

### 5.1.2 The Coupling Parameter and Transition Temperature

There is a theoretical calculate value of $\lambda \approx 0.7$.[1] The experimental value of the EPC in this TB-model is $\lambda \approx 0.6$, whilst the same DFT calculations indicate a value of $\lambda$ that is in the range of $[0.8, 1]$ which would give a $T_c$ in the range $[49, 72]$K. It is argued that in comparison with their result, this TB model resulted in a value around $T_c$ =23.2 K which is lower, although in Figure 15 our transition temperature maps to about the same values of $\lambda$. We assert that this gives validity to our model.

### 5.1.3 Superconductivity of Graphene with the Use of Doping

This is a theoretical viewpoint of the possibility of graphene's superconductivity. The process of lowering the Fermi level is essential for superconductivity and to take advantage of the high $\lambda$-value: One method available is hole doping.

Graphene is composed of graphene $^6$C. The simplest ways of manipulating the band structure by means of doping is with boron $^5$B or nitrogen and $^7$N. This corresponds to hole and electron doping, respectively.

By heavily doping graphene with 50% boron, one could hypothetically lower the Fermi energy to the top of the $\sigma$-bands of regular graphene. However by doping graphene with boron, other properties will be affected. According to a study by Jian Zhou et. al.[35], 50% bor-doped graphene is not dynamically stable at regular strain. It can be stabilised by applying a tensile strain and electron doping. The equilibrium lattice constant of this constellation is 2.677 Å, however by applying a tensile strain to increase the lattice constant by 5%, results in an effective lattice constant of 2.81085 Å. This procedure should hypothetically stabilise the composite material. [35]

In conclusion, doping graphene with boron is a future aspect of making it superconductive, although one must take in account the stabilisation of graphene.

## 5.2 Approximations in the Tight-Binding model

In this section, we will discuss the the approximations utilised in the model to the calculated the band structure, such as the nearest neighbour approximation and neglecting the overlap matrix.

### 5.2.1 Omitting the Next-Nearest Neighbour Hopping Integrals

A premise of this thesis is that the size of the error due to omitting all but the nearest neighbour integrals can be considered negligible, since the radial part of the wave functions falls off exponentially. According to a calculation examining the relative error between the nearest neighbour approximation (NNA) and the next-nearest neighbour approximation (NNNA) for the hopping parameter, this error is only one order of magnitude smaller[36], when two or three orders or higher would be preferred.

However, the band structure is qualitatively and quantitatively accurate around the high symmetry point $\bar{\Gamma}$ in an NN-approximation compared to DFT calculations [1]. The $\sigma$-band accuracy falls short around the $\bar{\text{M}}$- and $\bar{\text{K}}$-point, however these regions are not of interest in this thesis. The $\pi$-bands are accurate in the entire 1BZ, as they can be shown to be very much the same for fitted NN as for NNN up to the third nearest neighbour[37] even for $\mathbf{k}$ far from the Dirac point. This is

important in the interband scattering process. This suffice as reasons as to why this approximation is valid.

### 5.2.2 Neglecting Nearest Neighbour Overlap Integrals

When calculating the overlap integrals in the overlap matrix $S$ given by equation (57), this matrix is approximated as the identity matrix. In reality, the overlap between the orbitals aren't generally zero, as small overlap terms from distant sites sum up to possibly largely contributing overlaps. In this section, it is shown that these overlaps are small, and in the following sections, it is shown that the secular matrix is well-conditioned.

There are two cases of matrix overlaps in the interest of this section: where the orbitals originate on the same sites and where the orbitals originate on different sites. If the orbitals originate on the same atom, the NN-approximation removes any overlap, meaning that these are identically zero. This calculation is done by maximizing the sum over phase factors, i.e. taking the absolute value of the phase factors. When calculated for NNN using Slater type orbitals, the greatest contribution comes from

$$\left\langle 2p_x^{A1} \middle| 2p_x^{A2} \right\rangle \approx 3.5 \cdot 10^{-4} \tag{79}$$

meaning that the NN-approximation is valid regarding overlap between the same sites. Calculating the overlap integrals for orbitals on different NN-sites, also using Slater type orbitals, the greatest contribution comes from

$$\left\langle 2p_x^{A} \middle| 2p_x^{B} \right\rangle \approx 0.096 \tag{80}$$

which might actually pose a considerable problem if every contribution were of this magnitude. However, five elements has zero maximum contribution, five has $\approx 0.0013$ maximum contribution, and the rest has an average contribution of 0.0105. The $\left\langle 2s^A \middle| 2s^B \right\rangle$-contribution has a maximum contribution of less than three orders of magnitude. This calculation has only been done for $S_{AB}$, since $S_{BA} = S_{AB}^\dagger$, therefore considering all technicalities, there are twice as many terms. However since these values are relatively small, with the largest error being smaller than an order of magnitude and the median error being three orders of magnitude, it can be concluded that the overlap matrix approximated as the identity matrix is a valid approximation.

## 5.3 Slater Type Orbital Approximation

The Slater type orbitals are introduced in an attempt to correct for electron-electron interactions in the atom, which makes sense in a tight binding approximation where electrons are treated as tightly bound to their nucleus. The Slater

approximation is well suited for describing the orbital some distance away from the nucleus, as the approximation omits the radial nodes closer to the nucleus [12], but the only valence orbital in carbon with nodes is the $|2s\rangle$ orbital. The effect of including nodes would be that the value of the overlap integrals over different atoms would decrease, as the negative parts of the wave function for one atom is multiplied by the positive far field part of the other. The overlap of the $|2s\rangle$ orbitals in the Slater approximation is calculated in Section 5.2.2 to be less than 0.001, so any error introduced by omitting the nodes should have a very little effect on the overall calculations. It can be assumed that the error in the hopping parameters are of the same order, as they rely on the orbital overlap.

## 5.4 Condition Number of Transfer Matrix and Residuals

The condition number $\kappa$ of a matrix is a measurement of how sensitive the matrix $A$ is to changes in the input $x$.

$$Ax = b \tag{81}$$

The condition number is defined as a measure of the regularity of the matrix, such that

$$\kappa = \|A^{-1}\|\|A\|, \tag{82}$$

where a large $\kappa \gg 1$ depicts a more sensitive system, and $\kappa \approx 1$ means that the system is not sensitive to an error in input. The rule of thumb for the condition number is that the magnitude of the number determines how many digits of accuracy lost.

For this simulation the condition number $\kappa$ was in the range of $[6, 7.8]$ from the $\bar{\Gamma}$-point to the $\bar{K}$-point, which is an indication of a stable system. Taking Umklapp scattering into account the condition number is between $[2, 8]$. This indicates that the problem is well conditioned in the 1BZ.

Since there exists an analytical solution for the energy $\pi$-bands in graphene, it is possible to calculate the the difference between our results and the analytical answer, also called residuals. The calculated residuals are within
$[-2.4 \times 10^{-7}, 2.4 \times 10^{-7}]$ eV which are very small considering that the band energies are in the order of eV.

## 5.5 Single Major Contributing Phonon Mode Frequency to $\lambda$

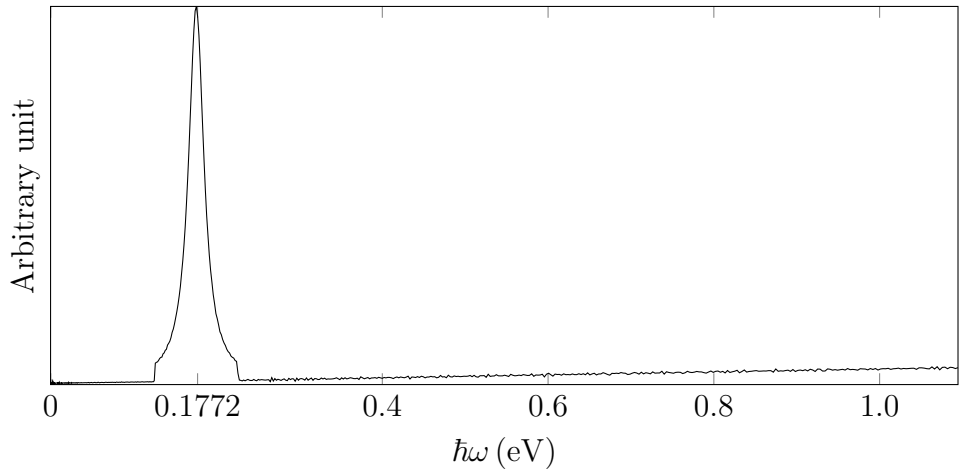


Figure 17: *Numerical derivative of the lifetime broadening* $\Gamma$ *with respect to energy. As made visible in the figure, there is a single dominant phonon frequency contribution to* $\Gamma$.

The $\lambda$-parameter can be calculated with equation (39) if there is a single dominant mode and frequency in the Eliashberg function. By derivation of the lifetime broadening with respect to frequency, or equally stated, with respect to energy(since energy is $\hbar$ multiplied by frequency), it is possible to obtain the Eliashberg function qualitatively, see equation (38). This yields the expression

$$\alpha^2 F_{n\mathbf{k}}(\omega) \propto \frac{\partial \Gamma_{n\mathbf{k}}}{\partial \varepsilon} \approx \frac{\Delta \Gamma_{n\mathbf{k}}}{\Delta \varepsilon} \tag{83}$$

In Figure 17, the numerically derived Eliashberg function is shown. This shows that there is indeed only a single dominant frequency in this function, meaning that equation (39) is indeed a good approximation near the $\Gamma$-point at the $\sigma$-bands. The lifetime broadening should in theory be derived for each contribution, however in this case it is clear that the derivation can be done without loss of generality. Therefore $\lambda$ can be calculated, yielding $\lambda$ approximatly $[0.5, 0.9]$.

## 5.6 Analysis of the Screening Parameter $\alpha$

The lifetime broadening $\Gamma$ in Section 4.1 depends on the chosen potential model $V(\mathbf{r})$ and on the chosen values of the model parameters. The chosen model potential takes the form of a Gaussian, see equation (71), with two parameters $V_0$

and $\alpha$. $V_0$ is the potential strength and $\alpha$ is the screening parameter, or potential attenuation in space. Since one of the core aims of the thesis is to study the lifetime broadening, it is valuable to investigate how sensitive $\Gamma$ is to changes in the potential parameters.

The perturbed potential that makes up the perturbed Hamiltonian is given by

$$\delta V_\nu(\mathbf{r}) = \frac{2V_0}{\alpha^2} e^{-(\frac{r}{\alpha})^2} \mathbf{r} \cdot \mathbf{Q}_\nu \tag{73}$$

and from the expanded lifetime broadening equation (68) and equation (69), it is easy to see that $\Gamma$ is directly proportional to $V_0^2$ for a constant value of $\mathbf{k}$. Changes made to $V_0$ are therefore not particularly interesting since it merely scales $\Gamma$ by a constant factor. $\alpha$ on the other hand, in addition to scaling $\Gamma$ by a factor of $\alpha^{-4}$, also affects the potential shape since it is a part of the exponent in equation (73). A change in $\alpha$ corresponds to a change in the physical properties of the system and is thus more interesting to analyse than $V_0$.

The value chosen for $\alpha$ is changed in increments from 1.20 a.u. to 1.80 a.u. corresponding to a $\pm 20\,\%$ change from our original value 1.50 a.u. In Figure 18 the total lifetime broadening $\Gamma$ is plotted for the original value of $\alpha$ and the two extremes $\pm 20\,\%$. Note that the photo hole energy is referenced from the top of the $\sigma_o$-band ($\varepsilon_\sigma$) so that the energy is really given by $\varepsilon_\sigma - \varepsilon_{n\mathbf{k}}$. $\Gamma$ attains maximum value for $\alpha = 1.50$ a.u. and minimum value for $\alpha = 1.20$ a.u. for all considered energies. The largest value of $\alpha$ will cause $\Gamma$ to lie in between the other two and will be more similar to $\Gamma_{\alpha=1.2}$ for lower energies and more similar to $\Gamma_{\alpha=1.5}$ for higher energies.

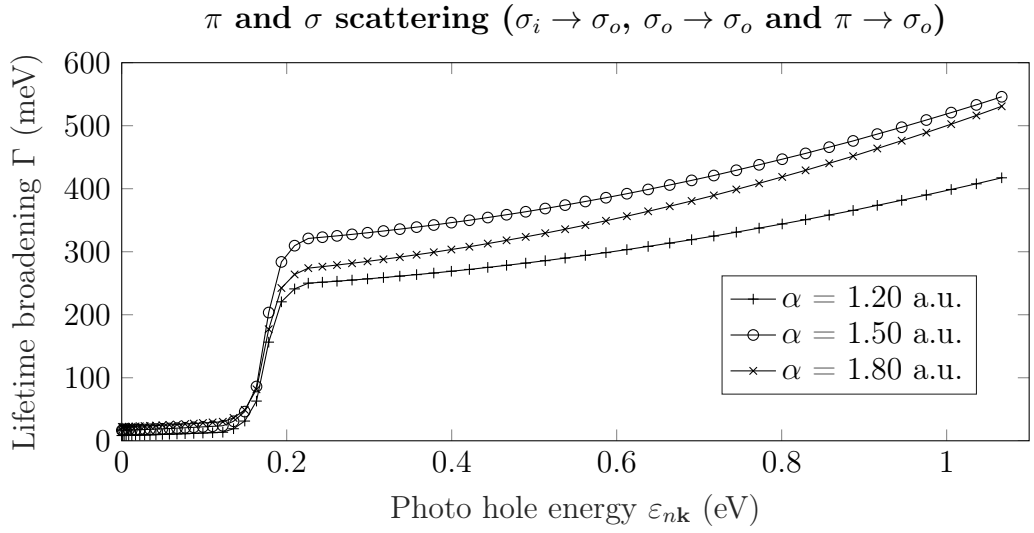


Figure 18: *The total lifetime broadening* $\Gamma$ *for three different values of the screening parameter* $\alpha$*. The photo hole energy is referenced from the top of the* $\sigma_o$*-band.*

In order to get a more detailed understanding it is helpful to plot $\Gamma$ against the different $\alpha$ values for a specific energy. This is done in Figure 19 for the total lifetime broadening ($\sigma$ and $\pi$ scattering) for $\varepsilon_{n\mathbf{k}} = 0.40\,\text{eV}$. Note that $\Gamma$ is strictly decreasing on both sides of a certain value of $\alpha$ that maximises it.

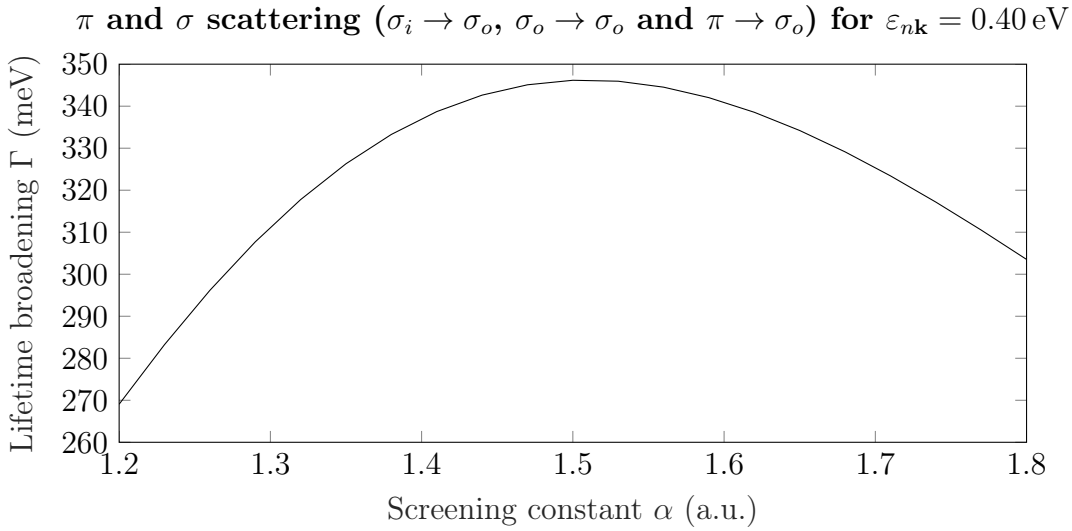


Figure 19: *The total lifetime broadening at photo hole energy* $\varepsilon_{n\mathbf{k}} = 0.40\,\text{eV}$ *for different values of the screening parameter* $\alpha$*.*

In the range $\alpha \in [1.2, 1.8]$ the lifetime broadening varies by 22 % relative to the maximum value for this specific energy, Similar numbers are obtained for other energy values after the kink at approximately 0.2 eV.

The $\sigma$ and $\pi$ scattering contributions can also be considered individually, see Figure 20a and Figure 20b respectively. The $\sigma$ scattering in Figure 20a shows a comparable $\alpha$ dependence to Figure 19 but the maximum is attained at a slightly lower $\alpha$. The $\pi$ scattering look different, but it is reasonable to suspect that a maximum will be reached at a larger $\alpha$ value than 1.8 a.u. Here, it is also possible to notice that the $\pi$ scattering seems to plays a significant part in the lifetime broadening, even though it is smaller than the $\sigma$ scattering contribution. This also seems to partly explain the behaviour in Figure 18 where $\Gamma_{\alpha=1.8}$ is similar to $\Gamma_{\alpha=1.5}$ for higher energies and similar to $\Gamma_{\alpha=1.2}$ for lower energies. The $\sigma$ scattering is attenuated for $\alpha = 1.8$ while $\pi$ scattering is maximised and for large energies this will be noticeable since $\Gamma_\pi$ grows faster than $\Gamma_\sigma$ after the kink in accordance with Figure 13a.

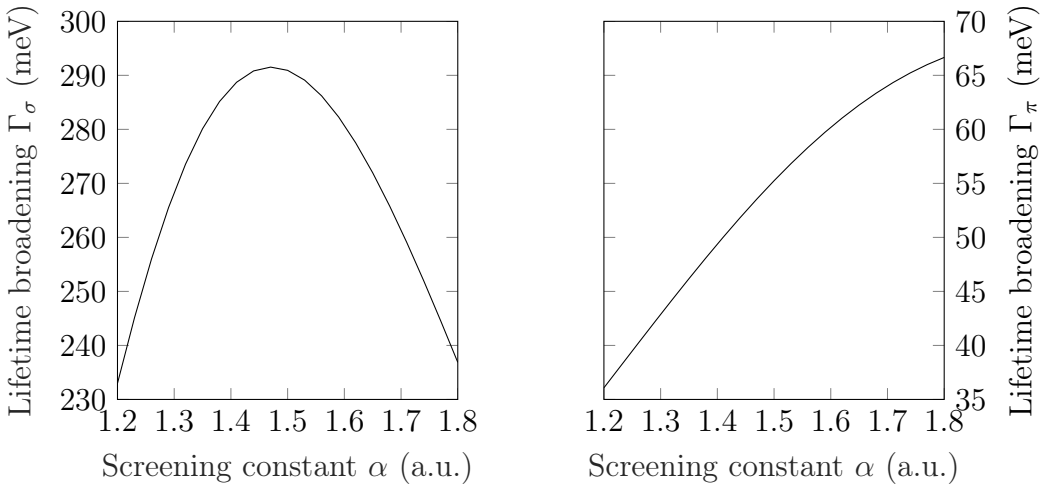


Figure 20: *The lifetime broadening at photo hole energy $\varepsilon_{n\mathbf{k}} = 0.40$ eV for different values of the screening parameter $\alpha$. $\sigma$ scattering ($\sigma_i \to \sigma_o$ and $\sigma_o \to \sigma_o$) is shown in a) and $\pi$ scattering ($\pi \to \sigma_o$) is shown in b).*

It is interesting that the lifetime broadening attains a maximum for a certain value of $\alpha$. Physically, $\alpha$ represents how widespread the potential is in space. A smaller $\alpha$ value will attenuate the potential while a larger value will increase its reach. If we consider the hopping $H'$ in equation (69) which $\Gamma$ is proportional to, we can see that in order for $H'$ to be nonzero the atomic orbitals and the perturbed potential must overlap in space. It then makes sense that $\Gamma$ decreases

for smaller $\alpha$ values since the overlap decreases. According to this argument, we might expect that $\Gamma$ increases as $\alpha$ grows indefinitely but as we have seen, it starts to decrease after a certain value. As noted in the beginning of this section $\Gamma$ is directly proportional to $\alpha^{-4}$ which means that larger $\alpha$ values also tends to decrease $\Gamma$ and for a large enough value this effect will dominate. The reverse effect does not take place for small $\alpha$ values since $\alpha^{-4}$ increases more slowly than the Gaussian decreases. It is therefore not strange that we see a maximum in $\Gamma$ for a certain $\alpha$.

The conclusion is that both potential parameters $V_0$ and $\alpha$ behave in a fairly predible way which may be seen as a sign of a consistent potential model.

# 6 Conclusion

The ARPES experimental data has a clear kink. We conclude that our simulated EPC gives a similar kink in the $\sigma$-band, compare with Figure 14a where the kink is very close to the measured spectral function superimposed in Figure 16. This result indicates that EPC is a major contributing phenomenon to the kink, as the simulated kink only relies on EPC, and not for example sublattice interference.

The relevant phonon modes are LO and TO for $\sigma$ scattering ($\sigma_i \to \sigma_o$ and $\sigma_o \to \sigma_o$) compared to $\pi$ scattering ($\pi \to \sigma_o$) where the relevant modes instead are ZO and ZA, where ZO is two orders of magnitude smaller than ZA. Both the $\sigma$ and the $\pi$ scattering processes are relevant and contribute to the lifetime broadening $\Gamma$ and therefore the spectral function. The $\pi$ scattering is as a consequence less important, as it makes up 10 % of $\Gamma$ at energies shortly after the kink, but still significant.

From $\Gamma$ the numerical simulations yielded $\lambda \approx 0.6$, which is below the experimentally measured $\lambda = [0.8, 1.0]$ from the ARPES, but in the range of the theoretical $\lambda \approx 0.7$ from [1]. The transition temperature was calculated to $T_c \approx 23.2\,\mathrm{K}$ from $\lambda$, which is at least 26 Kelvin lower than the expected $T_c$ from the experimentally obtained $\lambda$ values, but this is likely due to McMillan's formula for the temperature, which is highly sensitive to small changes in $\lambda$. This tells us that our TB model may not be as quantitatively reliable as DFT calculations, but viewed against the simulated kink it gives a satisfying qualitative result.

Most of the approximate models and formulas used in the thesis were evaluated, and especially the TB model was found to be sensitive to change in the potential parameters, where a change in the potential parameter $\alpha$ gave a change of results in $\Gamma$ of the same percentage. This behaviour is due to our choice of potential, and represents its reach.

In conclusion, graphene is not a natural superconductor because of the low density of states and low EPC of the $\pi$-band at the Fermi energy. The high density of states and the findings of strong EPC in the $\sigma$-band could motivate further research about lowering the Fermi energy to these bands. By doping graphene, it is theoretically possible to lower the $\sigma$-band to the Fermi level, and achieve superconductivity.

# Bibliography


[1] F. Mazzola, T. Frederiksen, T. Balasubramanian, P. Hofmann, B. Hellsing and J. W. Wells, 'Strong electron-phonon coupling in the $\sigma$ band of graphene', *Phys. Rev. B*, vol. 95, p. 075 430, 7 Feb. 2017. DOI: 10.1103/PhysRevB.95.075430. [Online]. Available: https://link.aps.org/doi/10.1103/PhysRevB.95.075430.

[2] F. Mazzola, 'Kinks in the $\sigma$ band of graphene induced by electron-phonon coupling.', *Physical Review Letters*, vol. 111, no. 216806, pp. 1–5, 2013. DOI: 10.1103/PhysRevLett.111.216806.

[3] F. Kusmartsev, W. Wu, M. Pierpoint and K. Yung, 'Application of graphene within optoelectronic devices and transistors', in *Applied Spectroscopy and the Science of Nanomaterials*, Springer, 2015, pp. 191–221.

[4] C. Lee, X. Wei, J. W. Kysar and J. Hone, 'Measurement of the elastic properties and intrinsic strength of monolayer graphene', *Science*, vol. 321, no. 5887, pp. 385–388, 2008, ISSN: 0036-8075. DOI: 10.1126/science.1157996. eprint: http://science.sciencemag.org/content/321/5887/385.full.pdf. [Online]. Available: http://science.sciencemag.org/content/321/5887/385.

[5] J. Wu, H. A. Becerril, Z. Bao, Z. Liu, Y. Chen and P. Peumans, 'Organic solar cells with solution-processed graphene transparent electrodes', *Applied Physics Letters*, vol. 92, no. 26, p. 263 302, 2008. DOI: 10.1063/1.2924771. eprint: http://dx.doi.org/10.1063/1.2924771. [Online]. Available: http://dx.doi.org/10.1063/1.2924771.

[6] D. Cohen-Tanugi and J. C. Grossman, 'Water desalination across nanoporous graphene', *Nano Letters*, vol. 12, no. 7, pp. 3602–3608, 2012, PMID: 22668008. DOI: 10.1021/nl3012853. eprint: http://dx.doi.org/10.1021/nl3012853. [Online]. Available: http://dx.doi.org/10.1021/nl3012853.

[7] A. A. Balandin, S. Ghosh, W. Bao, I. Calizo, D. Teweldebrhan, F. Miao and C. N. Lau, 'Superior thermal conductivity of single-layer graphene', *Nano Letters*, vol. 8, no. 3, pp. 902–907, 2008, PMID: 18284217. DOI: 10.1021/nl0731872. eprint: http://dx.doi.org/10.1021/nl0731872. [Online]. Available: http://dx.doi.org/10.1021/nl0731872.

[8] S. Bae, H. Kim, Y. Lee, X. Xu, J.-S. Park, Y. Zheng, J. Balakrishnan, T. Lei, H. Ri Kim, Y. I. Song, Y.-J. Kim, K. S. Kim, B. Özyilmaz, J.-H. Ahn, B. H. Hong and S. Iijima, 'Roll-to-roll production of 30-inch graphene films for transparent electrodes', *Nature Nanotechnology*, vol. 5, pp. 574–578, Aug. 2010. DOI: 10.1038/nnano.2010.132.

[9] S. W. Jung, W. J. Shin, J. Kim, L. Moreschini, H. W. Yeom, E. Rotenberg, A. Bostwick and K. S. Kim, 'Sublattice interference as the origin of $\sigma$ band kinks in graphene', *Phys. Rev. Lett.*, vol. 116, p. 186 802, 18 May 2016. DOI: 10.1103/PhysRevLett.116.186802. [Online]. Available: https://link.aps.org/doi/10.1103/PhysRevLett.116.186802.

[10] C. Kittel, *Introduction to Solid State Physics*, 8th ed. John Wiley & Sons, Inc., 2005, ISBN: 0-471-41526-X.

[11] B. B. C̃. Joachain, *Physics of Atoms and Molecules*, 2nd ed. Pearson Education Ltd., 1983, ISBN: 0-582-35692-X.

[12] J. Slater, 'Atomic shielding constants', *Physical Review*, vol. 36, pp. 57–64, 1930. DOI: https://doi-org.proxy.lib.chalmers.se/10.1103/PhysRev.36.57.

[13] R. Saito, G. Dresselhaus and M. Dresselhaus, in *Physical Properties of Carbon Nanotubes*. World Scientific, 1998, ch. 2, ISBN: 978-1-86094-093-4. [Online]. Available: http://app.knovel.com/hotlink/toc/id:kpPPCN0006/physical-properties-carbon/physical-properties-carbon.

[14] H. Ibach and H. Lüth, 'The electronic bandstructure of solids', in *Solid-State Physics: An Introduction to Principles of Materials Science*. Berlin, Heidelberg: Springer Berlin Heidelberg, 2009, pp. 159–189, ISBN: 978-3-540-93804-0. DOI: 10.1007/978-3-540-93804-0_7. [Online]. Available: http://dx.doi.org/10.1007/978-3-540-93804-0_7.

[15] B. Gharekhanlou and S. Khorasani, *An overview of tight-binding method for two-dimensional carbon structures: Graphene: Properties, synthesis and applications*, Z. Xu, Ed. Nova Science Publishers, Inc., 2011, pp. 1–36, ISBN: 978-1-61470-949-7. [Online]. Available: http://sina.sharif.edu/~khorasani/Publications/Graphene.pdf.

[16] L. Lou, *Introduction to Phonons and Electrons*. River Edge: World Scientific Publishing Company, 2003, ISBN: 981-238-439-1. [Online]. Available: http://ebookcentral.proquest.com/lib/chalmers/detail.action?docID=1681614 (visited on 10/05/2017).

[17] L. S. Hampus Torén, 'Kvalitativ analys av elektron-fonon-kopplingen i grafen', pp. 1–30, 2015.

[18] P. A. M. Dirac, 'The quantum theory of the emission and absorption of radiation', *Proceedings of the Royal Society of London A: Mathematical, Physical and Engineering Sciences*, vol. 114, no. 767, pp. 243–265, 1927, ISSN: 0950-1207. DOI: 10.1098/rspa.1927.0039. eprint: http://rspa.royalsocietypublishing.org/content/114/767/243.full.pdf. [On-

line]. Available: http://rspa.royalsocietypublishing.org/content/114/767/243.

[19] J. O. Fjærestad. (2013). Introduction to green functions and many-body perturbation theory. [Online, accessed 2017-04-08], [Online]. Available: folk.ntnu.no/johnof/green-2013.pdf.

[20] B. Moritz. (2014). Devereaux group: Arpes, [Online]. Available: https://web.stanford.edu/group/photontheory/ARPES.html (visited on 08/04/2017).

[21] Wikipedia. (2016). Angle-resolved photoemission spectroscopy — wikipedia, the free encyclopedia. [Online; accessed 8-April-2017], [Online]. Available: https://en.wikipedia.org/w/index.php?title=Angle-resolved_photoemission_spectroscopy&oldid=730153478.

[22] B. Hellsing, A. Eiguren and E. Chulkov, 'Electron-phonon coupling at metal surfaces', *Journal of Physics: Condensed Matter*, vol. 14, no. 24, p. 5959, 2002. [Online]. Available: http://iopscience.iop.org/article/10.1088/0953-8984/14/24/306/pdf.

[23] J. Vinson, T. Jach, M. Müller, R. Unterumsberger and B. Beckhoff, 'Quasiparticle lifetime broadening in resonant x-ray scattering of $NH_4NO_3$', *Phys. Rev. B*, vol. 94, p. 035 163, 3 Jul. 2016. DOI: 10.1103/PhysRevB.94.035163. [Online]. Available: https://link.aps.org/doi/10.1103/PhysRevB.94.035163.

[24] A. Damascelli, Z. Hussain and Z.-X. Shen, 'Angle-resolved photoemission studies of the cuprate superconductors', *Rev. Mod. Phys.*, vol. 75, p. 479, 2 Apr. 2003. DOI: 10.1103/RevModPhys.75.473. [Online]. Available: https://link.aps.org/doi/10.1103/RevModPhys.75.473.

[25] B. Y. Hu, 'Kramers–kronig in two lines', *American Journal of Physics*, vol. 57, no. 9, pp. 821–821, 1989. DOI: 10.1119/1.15901. eprint: http://dx.doi.org/10.1119/1.15901. [Online]. Available: http://dx.doi.org/10.1119/1.15901.

[26] G. A. Ummarino, 'Eliashberg theory, from emergent phenomena in correlated matter modeling and simulation, vol. 3', in. Verlag des Forschungszentrum, Jul. 2013, ch. 13.2.2, ISBN 978-3-89336-884-6.

[27] H. Kamerlingh-Onnes, 'On the sudden change in the rate at which the resistance of mercury disappears', *Comm. Phys. Lab. Univ. Leiden*, p. 124, 1911.

[28] Y. S. Jain, 'First quantization and basic foundation of the microscopic theory of superconductivity', *Journal of Applied and Fundamental Sciences*, vol. 2, no. 2, p. 78, 2016.

[29] A. Drozdov, M. Eremets, I. Troyan, V. Ksenofontov and S. Shylin, 'Conventional superconductivity at 203 kelvin at high pressures in the sulfur hydride system', *Nature*, vol. 525, no. 7567, pp. 73–76, 2015.

[30] P. B. Allen and R. Dynes, 'Transition temperature of strong-coupled superconductors reanalyzed', *Physical Review B*, vol. 12, no. 3, p. 905, 1975. DOI: 10.1103/PhysRevB.12.905. [Online]. Available: https://link.aps.org/doi/10.1103/PhysRevB.12.905.

[31] B. Hellsing, Personal discussions, 2017.

[32] I. Pletikosi ć, M. Kralj, M. Milun and P. Pervan, 'Finding the bare band: Electron coupling to two phonon modes in potassium-doped graphene on ir(111)', *Phys. Rev. B*, vol. 85, p. 155 447, 15 Apr. 2012. DOI: 10.1103/PhysRevB.85.155447. [Online]. Available: https://link.aps.org/doi/10.1103/PhysRevB.85.155447.

[33] D. M. Gaitonde, P. Modak, R. S. Rao and B. K. Godwal, 'Electronic structure and superconductivity of mgb2', *Bulletin of Materials Science*, vol. 26, no. 1, pp. 137–141, 2003, ISSN: 0973-7669. DOI: 10.1007/BF02712801. [Online]. Available: http://dx.doi.org/10.1007/BF02712801.

[34] C. Si, Z. Liu, W. Duan and F. Liu, 'First-principles calculations on the effect of doping and biaxial tensile strain on electron-phonon coupling in graphene', *Physical review letters*, vol. 111, no. 19, p. 196 802, 2013. DOI: 10.1103/PhysRevLett.111.196802. [Online]. Available: https://link.aps.org/doi/10.1103/PhysRevLett.111.196802.

[35] J. Zhou, Q. Sun, Q. Wang and P. Jena, 'High-temperature superconductivity in heavily n-or b-doped graphene', *Physical Review B*, vol. 92, no. 6, p. 064 505, 2015.

[36] J.-N. Fuchs and M. O. Goerbig, 'Introduction to the physical properties of graphene', *Lecture Notes*, 2008.

[37] A. Bostwick, T. Ohta, J. L. McChesney, T. Seyller, K. Horn and E. Rotenberg, 'Band structure and many body effects in graphene', *The European Physical Journal-Special Topics*, vol. 148, no. 1, pp. 5–13, 2007.

[38] M. E. Peskin, D. V. Schroeder and E. Martinec, *An introduction to quantum field theory*, 1996.

[39] J. Bauer, J. E. Han and O. Gunnarsson, 'The theory of electron–phonon superconductivity: Does retardation really lead to a small coulomb pseudopotential?', *Journal of Physics: Condensed Matter*, vol. 24, no. 49, p. 492 202, 2012.

# A The Transfer Matrix Elements

Here we detail the elements of the transfer matrix $H$, in Section 3.3, as presented in for example [15].

## A.1 The $\sigma$-band Transfer Matrix

With the nearest neighbour approximation we get three $\mathbf{R}_{Ai}$ vectors, seen in figure 8, given by

$$\mathbf{R}_{A1} = a\left(\frac{-1}{\sqrt{3}}, 0\right), \quad \mathbf{R}_{A2} = a\left(\frac{1}{2\sqrt{2}}, \frac{\sqrt{3}}{2\sqrt{2}}\right), \quad \mathbf{R}_{A3} = a\left(\frac{1}{2\sqrt{2}}, -\frac{\sqrt{3}}{2\sqrt{2}}\right). \quad (84)$$

By dividing up the wave function into its orbital components according to the method described in Section 3.2, the elements may be calculated as

$$\left\langle 2s^A \right| \hat{H} \left| 2s^B \right\rangle = H_{ss\sigma} \sum_{i=1}^{3} e^{i\mathbf{k}\cdot\mathbf{R}_{Ai}} \quad (85)$$

$$\left\langle 2s^A \right| \hat{H} \left| 2p_x^B \right\rangle = H_{sp\sigma} \sum_{i=1}^{3} e^{i\mathbf{k}\cdot\mathbf{R}_{Ai}} \cos\theta \quad (86)$$

$$\left\langle 2s^A \right| \hat{H} \left| 2p_y^B \right\rangle = H_{sp\sigma} \sum_{i=1}^{3} e^{i\mathbf{k}\cdot\mathbf{R}_{Ai}} \sin\theta \quad (87)$$

$$\left\langle 2p_x^A \right| \hat{H} \left| 2p_x^B \right\rangle = \sum_{i=1}^{3} (H_{pp\sigma} \cos^2\theta + H_{pp\pi}(1 - \cos^2\theta)) e^{i\mathbf{k}\cdot\mathbf{R}_{Ai}} \quad (88)$$

$$\left\langle 2p_y^A \right| \hat{H} \left| 2p_x^B \right\rangle = \sum_{i=1}^{3} (H_{pp\sigma} - H_{pp\pi}) \cos\theta \sin\theta e^{i\mathbf{k}\cdot\mathbf{R}_{Ai}} \quad (89)$$

$$\left\langle 2p_y^A \right| \hat{H} \left| 2p_y^B \right\rangle = \sum_{i=1}^{3} (H_{pp\sigma} \sin^2\theta + H_{pp\pi}(1 - \sin^2\theta)) e^{i\mathbf{k}\cdot\mathbf{R}_{Ai}}, \quad (90)$$

where the rest of elements can be calculated by the fact that $\langle i| \hat{H} |j\rangle = \langle j| \hat{H} |i\rangle^\dagger$, where $^\dagger$ is the Hermitian transpose.

## A.2 The $\pi$-band Transfer Matrix

Just like in the previous section, the transfer matrix element of the $\pi$-band can be calculated as

$$\left\langle 2p_z^A \right| \hat{H} \left| 2p_z^B \right\rangle = H_{pp\pi} \sum_{i=1}^{3} e^{i\mathbf{k}\cdot\mathbf{R}_{Ai}} \quad (91)$$

where the other element is the Hermitian transpose of equation (91).

# B Migdal-Eliashberg Theory

Superconductivity is an emergent phenomenon at low temperatures due to the quantum nature of materials. According to Bardon-Cooper-Schrieffer(BCS) theory, superconductivity is a phase and can thus be modelled as one. Due to some effects observed such as the Meissner effect and changes in the thermodynamical properties of the superconducting state, this suggests a band gap at the Fermi level, which back then was surprising due to the Pauli exclusion principle. This is accredited due to the formation of Cooper pairs, two electrons bound together becoming a single boson. BCS theory treats this and arrives at the equation

$$E_{\mathbf{k}} = \sqrt{\varepsilon_{\mathbf{k}}^2 + \Delta_{\mathbf{k}}^2} \tag{92}$$

for the Cooper pair energy, where $\varepsilon_{\mathbf{k}}$ is the electron energy dispersion, and $\Delta_{\mathbf{k}}$ is defined as the gap function, which has a dependency of temperature and tends to zero when $T \to T_c$. However, the BCS theory yields good results only for low temperature superconductors, and via *Migdal-Eliashberg theory*, a better approximation of the transition temperature can be realised.

In this section, the Green function formalism behind the *Eliashberg equations* will be treated briefly. These equations lay another foundation of the theory behind the superconducting state, and more precisely yields an equation describing the superconducting band gap. This in turn gives an approximation of the transition temperature of the superconducting state. The Eliashberg function $\alpha^2 F$ as well as the EPC-parameter $\lambda$ occurs naturally through this derivation, however neither these nor the entire derivation of McMillan's formula will not be treated here; it serves the purpose of giving insight into how complicated these systems actually are.

There's lots of new concepts in this chapter. Beginning at *Nambu formalism*, which is simply put a 2-component electron wavefunction consisting of the different spins, a phonon field operator consisting of the creation and the annihilation operator for phonons, and a rather lengthy Hamiltonian, one obtains two Green functions. One for the electron denoted $G$ and one for the phonon denoted $D_\nu$. These can be expanded in Fourier series over the *Matsubara frequencies*, yielding

$$\begin{aligned} G(\mathbf{k}, \tau) &= \frac{1}{\beta} \sum_{n=-\infty}^{\infty} e^{-i\omega_n \tau} G(\mathbf{k}, i\omega_n) \\ D_\nu(\mathbf{q}, \tau) &= \frac{1}{\beta} \sum_{n=-\infty}^{\infty} e^{-i\nu_n \tau} D(\mathbf{q}, i\nu_n). \end{aligned} \tag{93}$$

where $\nu$ is a phonon mode, $\nu_n$ are the boson Matsubara frequencies and $\omega_n$ are the fermion Matsubara frequencies. The Matsubara frequencies aren't dangerous; if a Green function $g(\omega)$ for an interaction is given at 0 Kelvin, the Green function at a finite temperature is the sum over all $g(i\omega_n)/\beta$ where $\omega_n$ are the Matsubara frequencies and $\beta = \hbar/k_B T$.

The one-electron non-interacting Green function becomes

$$G_0(\mathbf{k}, i\omega_n) = [i\omega_n \mathbb{I} - \varepsilon_{\mathbf{k}}\sigma_3]^{-1} \tag{94}$$

where $\varepsilon_{\mathbf{k}}$ is the one-electron Bloch energy relative to the Fermi level and $\sigma_3$ is the third Pauli spin matrix. Pauli spin matrices are used since they are hermitian, unitary, and form a basis of $2\times2$-matrices together with the identity matrix. The phonon non-interacting Green function is

$$D_0(\mathbf{q}, i\nu_n) = [M(\omega^2(\mathbf{q}) - \nu_n^2)]^{-1} \tag{95}$$

where $M$ is the ion mass and $\omega(\mathbf{q})$ is the phonon dispersion relation. By analysing Feynman diagrams, a *Dyson*-like equation for the electron and phonon Green functions is obtained:

$$\begin{aligned} [G(\mathbf{k}, i\omega_n)]^{-1} &= [G_0(\mathbf{k}, i\omega_n)]^{-1} - \Sigma(\mathbf{k}, i\omega_n) \\ [D_\nu(\mathbf{q}, i\omega_n)]^{-1} &= [D_{0,\nu}(\mathbf{q}, i\omega_n)]^{-1} - \Pi(\mathbf{k}, i\omega_n) \end{aligned} \tag{96}$$

where $\Sigma$ and $\Pi$ are the electron and the phonon self-energies respectively. There is a theorem called *Migdal's theorem*, which states that any *vertex correction* are of size $\mathcal{O}(\sqrt{m/M})$, where $m$ is the electron mass. Vertex corrections are exactly what they sound like; a correction to an interaction vertex, analogous to the way a perturbation is a correction to a Hamiltonian[38]. Thus only the bare vertex is considered. The electron self-energy will thus be approximated as

$$\Sigma(\mathbf{k}, i\omega_n) = -\frac{1}{\beta}\sum_{\mathbf{k}'n'\nu} \sigma_3 G(\mathbf{k}', i\omega_{n'})\sigma_3 \left[|g_{\mathbf{k}\mathbf{k}'\nu}|^2 D_\nu(\mathbf{k}-\mathbf{k}', i\omega_n - i\omega_{n'}) + V_c(\mathbf{k}-\mathbf{k}')\right] \tag{97}$$

where $V_c$ is the screened Coulomb potential. We may rewrite equation (97) on the basis consisting of the Pauli matrices and the identity matrix,

$$\Sigma(\mathbf{k}, i\omega_n) = i\omega_n[1 - Z(\mathbf{k}, i\omega_n)]\mathbb{I} + \chi(\mathbf{k}, i\omega_n)\sigma_3 + \phi(\mathbf{k}, i\omega_n)\sigma_1 + \overline{\phi}(\mathbf{k}, i\omega_n)\sigma_2 \tag{98}$$

where the new functions $Z$, $\chi$, $\phi$, and $\overline{\phi}$ has been introduced and defined. Now, the Dyson-like equation (96) can be used to replace the self-energy in the equation above, yielding

$$[G(\mathbf{k}, i\omega_n]^{-1} = i\omega_n Z\mathbb{I} - (\varepsilon_{\mathbf{k}} + \chi)\sigma_3 - \phi\sigma_1 - \overline{\phi}\sigma_2 \tag{99}$$

Inverting this matrix gives

$$G(\mathbf{k}, i\omega_n) = \frac{1}{\Theta}[i\omega_n Z\mathbb{I} + (\varepsilon_{\mathbf{k}} + \chi)\sigma_3 + \phi\sigma_1 + \overline{\phi}\sigma_2] \\ \frac{1}{\Theta}\begin{bmatrix} i\omega_n Z + (\varepsilon_{\mathbf{k}} + \chi) & \phi - i\overline{\phi} \\ \phi + i\overline{\phi} & i\omega_n Z - (\varepsilon_{\mathbf{k}} + \chi) \end{bmatrix} \tag{100}$$

where $\Theta$ is the determinant

$$\Theta = (i\omega_n Z)^2 - (\varepsilon_{\mathbf{k}} + \chi)^2 - \phi^2 - \overline{\phi}^2 \tag{101}$$

Section 2.5 In section Section 2.5, the spectrum of the Green function was given by the imaginary part of it. This yielded peaks at the poles of the Green function; the electron excitations were given by where the pole was. Using this analogy, the elementary electron excitations of the rather more complicated system here are given by where $\Theta = 0$. However, this would yield imaginary energies, which is typically unphysical. Some complex analysis can be utilized to analytically continue the Green function[1] giving $G(\mathbf{k}, \omega)$, and its elementary excitations are given by $\Theta = 0$. This yields (in atomic units)

$$E_{\mathbf{k}} = \sqrt{\left(\frac{\varepsilon_{\mathbf{k}} + \chi}{Z}\right)^2 + \frac{\phi^2 + \overline{\phi}^2}{Z^2}}. \tag{102}$$

This equation is of a familiar form; just like the gap equation predicted by the BCS theory. By explicitly writing out the expression for the self-energy in terms of the equations $Z$, $\chi$, $\phi$, and $\overline{\phi}$ together with the equation

$$n = 1 - \frac{2}{\beta}\sum_{\mathbf{k}'n'} \frac{\chi(\mathbf{k}', i\omega_{n'}) + \varepsilon_{\mathbf{k}'}}{\Theta(\mathbf{k}', i\omega_{n'})}, \tag{103}$$

where $n$ is the electron density, one arrives at the Eliashberg equations. The electron density can be used to calculate the chemical potential $\mu$. This set of equations can be used to describe the superconducting state in a broader sense. Delving further into these equations one can utilise the definition of the Eliashberg function and the EPC-parameter $\lambda$ to describe them, and by simplification, one obtains a relatively simple equation for the transition temperature $T_c$. This was the case for McMillan, who after simplification fitted parameters to a large set of data utilising the spectral function for lead and fitted the data for $\lambda < 2$ and $\mu^* < 0.15$, where

$$\mu^* = \frac{\mu}{1 + \mu\ln(E_{el}/\omega_{ph})}. \tag{104}$$

[1] Analytic continuation is an ill-posed problem in mathematics, however it does present a result here.

[39] Here, $E_{el}$ and $\omega_{ph}$ are 'typical' electron and phonon energies. The formula is

$$T_c = \frac{\Theta_D}{1.45} \exp\left\{ -\frac{1.04(1+\lambda)}{\lambda - \mu^*(1+0.62\lambda)} \right\} \tag{105}$$

where $\Theta_D$ is the Debye temperature. In 1975, this formula was found to be "highly accurate for all known materials with $\lambda < 1.5$" according to P. B. Allen and R. C. Dynes[30].

# C Bidragsrapport

## C.1 Ansvarsområden

Vi delade upp kandidatgruppen i två ansvarsområden, teorigrupp och proggrammeringsgrupp, där Oskar, Henrik och Kristofer ansvarade för de teoretiska, och litterära områdena i rapporten, emedan Victor, Timothy och Andreas koncentrerade sig på programmering, simulering, metod och den teorihämtning som var mest relevant för programmeringen. Överlappet mellan grupperna var väldigt litet, med undantag för att programmeringsgruppen ansvarade för den teori som var mest relevant för deras beräkningar.

Informationsinhämtning gjordes till stor del av litteraturstudier. Litteraturen utgjordes i huvudsak av kurslitteratur, kursanteckningar vid olika universitet, samt sist men inte minst vår handledares Bo genomgångar. Den sistnämnda av synnerligen intresse för programmeringsgruppen. För förståelsens skull anordnades två möten där FORTRAN presenteras för resten av gruppen.

Metoderna vidareutvecklades från handledarens kod.

## C.2 Bidrag till problemlösning

Algoritmer och den huvudsakliga implementeringen av nya funktioner sköttes av Victor. Ett avgörande problem för arbetet var beräkningen av spektralfunktionen och Kramer-Krönig-transformen (KK) numeriskt. Victor ansvarade för att skriva algoritmerna för dessa, vilket visade sig mer utmanande än väntat. KK-transformen är icke-konvergent, och därför undersöktes flera olika algoritmer: MacLaurin-summering, dubbel fast-fourier-transform, samt slutligen en kombination via hilbert-transformen.

Vidare implementerade Victor också spektralfunktionen, som är ett skalärt fält som renormaliserar ett band. Det gjordes flera iterationer av spektralfunktionen, men ingen tycktes matcha förväntningen. Förståelsen för denna rent numeriskt var inte helt klar för handledaren. Victor och Timothy spenderade en lång tid för att reda ut ny teori i spektralfunktionen för att slutföra algoritmen.

En vidare förutsättning för spektralfunktionsalgoritmen var partikel-hålsymmetrin i livstidsbreddningen. Detta var känt av vår handledare, men han valde att undanhålla detta för gruppen i hopp om att vi skulle nå samma slutsats. Victor och Andreas insåg att det fanns ett krav av symmetri i livstidsbreddningen för att producera självenergin utan singulariteter i ändpunkterna.

En stor diskussion som instigerades av teorigruppen var en effektivisering av algoritmen för EPC-matriselementet. Kristofer föreslog att man kunde dela upp Brillouin-zonen i 12 lika delar och beräkna i endast en av dem. Handledaren upptäckte emellertid att detta skulle kräva att man tog i beaktande fasen på ett lite mer invecklat sätt, men det bidrog till förståelsen av kod och teori för gruppen, samt en framtida effektivisering.

Gruppdiskussioner var essentiella för gruppens framskridande, och alla deltog lika mycket inom undergrupperna. En stor del av reflektion och kontroll av förståelsen var tack vare Timothy. Han spenderade mycket tid på att i detalj sätta sig in i kod och teori för att kunna kontrollera övrigas förståelse. Vi etablerade i början att förändringar i rapporten av innehållsart krävde konsensus, en princip vi hållit oss till.

## C.3 Redaktionell ansvarsfördelning

En konsekvens av gruppindelningen är att vissa avsnitt har haft huvudförfattare från teori- eller programmeringsgruppen som huvudförfattare. Teorigruppen har nästan uteslutande ansvarat för introduktion, sammandrag och teori. Syftet är i huvudsak skrivet av Timothy. Diskussionen är skriven av hela gruppen.

I teorigruppen har diskussionerna handlat mycket om vår grundläggande modell och EPC. Vad gäller NN-approximationen har Oskar, Kristofer och Victor fört diskussionen framåt, emedan EPC redits ut av i synnerhet Kristofer och Timothy.

Oskar har arbetat intensivt för förståelsen av den komplexa teorin bakom supraledning och den så kallade Migdal-Eliashberg-formalismen i appendix. Som konsekvens har han varit huvudförfattare för avsnitten om Eliashberg-teori. Oskar har också ansvarat för Greens-formalismen bakom spektralfunktionen, samt varit huvudförfattare för följande avsnitt:

- 2.1.4, 2.2, 2.5, 2.5.1, 2.5.2, 2.6, 2.7, 5.2, 5.2.1, 5.2.2, 5.3(med Kristofer), 5.5, A.2, B

Henriks fokus har varit introduktion, fononer, EPC, dopning och supraledning. Som konsekvens har han ansvarat för stora delar av den centrala litteratursökningen tillsammans med Kristofer. Han har varit huvudförfattare för de kapitel som hanterar i synnerhet supraledning och temperaturer i teori, resultat och diskussion. Han har huvudförfattat följande kapitel:

- 2.2, 2.4 (med Kristofer och Victor), 2.3 (med Victor), 2.7, 4.2, 5.1.2

Kristofer har ansvarat fullständigt för allt redaktionärt, organisatoriskt och litterärt i rapporten. Han har varit huvudsklig sekreterare vid våra möten och således författat våra mötesprotokoll. Han har varit huvudförfattare för och många av de tidiga avsnitten i teorin.

- 2.1.1, 2.1.2 (andra halvan Victor), 2.1.3, 2.1.4, 2.4 (med Henrik och Victor), 5.3 (med Oskar), abstract (med Andreas), svensk sammanfattning (Problemkapitlet samt korrektioner med Andreas), titelblad och tryckortssida, formatering av hela rapporten, all filstruktur på sharelatex

Programmeringsgruppen har själv skrivit metoden, och bidragen från teorigruppen har varit mestadels redaktionella.

Timothy har än en gång sett till att övriga programmeringsgruppen, Andreas och Victor har haft ordentlig koll på vad som faktiskt händer, och inte tvekat att rätta oss. Han fördjupade sig i koden och ämnet och gav ofta reflektioner och invändningar, vars nytta inte kan sättas i ord. Timothy har också haft vissa huvudsakliga författarskap, nämligen

- 5.6 Diskussion - $\alpha$, 5.4 Diskussion - kondition och residual, 3.1 Metod - TB-modell och NNA, 1.3 Introduktion - syfte och omfattning av arbetet

Timothy gjorde också en bild om grafenstruktur, samt de bilderna i 5.6.

Det huvudsakliga arbetet från Andreas redaktionellt har varit konsekvenstänkande och korrektioner. Han såg till att det fanns en röd tråd genom hela rapporten och att vi återkopplade väl till syftet. Detta har varit ovärderligt för ett konsistent arbete. Andreas hade också två möten om just FORTRAN i syfte att lära de övriga programmeringsspråket han lätt fick försprång i. Hans skriftliga bidrag har varit i synnerhet i

- 3.2, 5.4 Diskussion - kondition och residual, abstract (med Kristofer) A.1, svensk sammanfattning (Metodkapitlet samt korrektioner med Kristofer),

Victor ansvarade för stora delar av algoritmiseringen och därför även de delarna av metoden som svarar mot detta, samt resultatet av metoderna och diskussionen av resultatet. Han gjorde också all grafik och bilder i rapporten, med undantag för ett antal få. Alla bilder är egengjorda utom en, och kräver därför ingen särskild hänvisning eller källa.

- 2.1.2 (första halvan Kristofer), 2.3 (med Henrik), 2.4.1 (med Henrik och Kristofer), 2.5, 2.5.1, 3.2, 3.3, 3.4, 3.5, 4.1, 5.1.2, 5.2 A.1

## C.4 Sammanfattning och slutsats

Det är gruppens åsikt att arbetet varit någorlunda väl fördelat, så när som individuella ambitioner. Vi är väldigt nöjda med gruppen som helhet och våra prestationer under halvåret tillsammans, och hoppas det avspeglas i rapporten.